ELSEVIER

Journal of Structural Geology 29 (2007) 166–188

JOURNAL OF STRUCTURAL GEOLOGY

www.elsevier.com/locate/jsg

Geometry, kinematics and deformation rates along the active normal fault system in the southern Apennines: Implications for fault growth

Ioannis D. Papanikolaou, Gerald P. Roberts*

The Research School of Earth Sciences, Birkbeck College and University College London, Gower Street, London WC1E 6BT, UK

Received 10 January 2005; received in revised form 1 July 2006; accepted 14 July 2006
Available online 4 October 2006

Abstract

Throw rates, throws and kinematic data have been collected from a localised system of active normal faults in the southern Apennines, Italy, to assess how its growth history differs from that for a distributed fault system in the central Apennines. Both show evidence for fault interaction in that (1) faults located centrally along strike have higher throws and throw rates than distal faults, and (2) cumulative throw and throw-rate profiles summed across strike show central maxima with values decreasing to zero at fault system tips. However, although throw rates increased through time in the central Apennines, we are unable to resolve such changes if they exist for the southern Apennines. Specifically, throw rates derived from offsets of 18 ka geomorphic surfaces are consistent with total throws in the southern Apennines when extrapolated back through time, but overestimate total throws in the central Apennines by a factor of 2.4, suggesting an increase in throw-rate through time for the latter. We discuss why some fault systems appear to have throw rates that are constant through time whilst others accelerate during growth/interaction.

Keywords: Active normal fault; Fault growth; Fault interaction; Earthquake; Italy

1. Introduction

Slip-rate histories on normal fault systems are a fundamental constraint on continental deformation because they control earthquake recurrence intervals and provide a timescale for processes responsible for basin formation and lithospheric thinning. Recently, observations of natural fault systems have shown that for some, slip rates change through time due to interaction during fault growth (McLeod et al., 2000; Roberts et al., 2002; Chevalier et al., 2003; Roberts and Michetti, 2004; Taylor et al., 2004; Cowie et al., 2005) (Fig. 1). Specifically, as faults increase in size and accommodate more strain per unit time, some faults within a system cease to be active whilst slip rates on others increase to maintain constant regional strain rates. Fault dimensions and the positions of active faults evolve until late in the faulting history in these examples (up to 75% of the rifting history; Roberts and Michetti, 2004; Cowie et al., 2005). These observations are consistent with numerical models of fault growth, and growth histories suggested by observations of scaling between fault lengths and displacements during growth by propagation, linkage and interaction (Cartwright et al., 1995; Cowie, 1998; Cowie and Roberts, 2001). However, observations of other fault systems suggest that slip rates are essentially constant through time (Nicol et al., 1997; Walsh et al., 2001, 2002; Meyer et al., 2002). Fault patterns were established early in the faulting history in these examples (e.g. within the first 18–19% of the rifting history; Walsh et al., 2002). These conflicting findings lend uncertainty to understanding of processes responsible for basin formation, lithospheric thinning and seismic hazard. If the above variations are real, it would help to know what controls such variation in slip-rate histories.

* Corresponding author.
E-mail address: gerald.roberts@ucl.ac.uk (G.P. Roberts).

0191-8141/$ - see front matter © 2006 Elsevier Ltd. All rights reserved.
doi:10.1016/j.jsg.2006.07.009

In this paper we investigate the throw-rate history (vertical component of slip rate) of an active normal fault system in southern Italy, and show that we cannot resolve an increase in throw-rate through time or death of large, basin-bounding faults across strike. We choose this example because, in contrast, throw rates in the central Apennines increased in the Mid-Upper Pleistocene (Cavinato et al., 2002; Roberts et al., 2002; Roberts and Michetti, 2004), coincident with death of large basin-bounding faults neighbouring the Tyrrhenian coast (Fig. 1a); extension was distributed across the Apennines and the Tyrrhenian coastal plain prior to this time (Cavinato and De Celles, 1999; Galadini and Messina, 2004). As the central and southern Apennines share tectonic histories and lithospheric structure, the difference between them cannot be explained in this way. However, we note that the fault systems have different geometries (Fig. 1a), and the southern Apennines has higher heat flow (Minissale, 2004; see below for details). Our aim is to document the growth history of the fault system in the southern Apennines, and discuss why it differs from that in the central Apennines.

2. Geological background

The Apennines are part of the Alpine orogenic system that formed as a result of the subduction of Tethyan ocean crust and collision between African continental fragments and the Eurasian plate (Doglioni et al., 1996). During the Upper Miocene–Lower Pliocene, extension and accretion of new oceanic crust occurred in the Tyrrhenian Sea west of Italy (Lucente et al., 1999). Active subduction of the Ionian sea beneath Calabria was occurring at the same time with a progressive eastward migration of compressional fronts (Malinverno and Ryan, 1986). Pliocene rocks have been encountered in wells penetrating carbonate thrust sheets in the southern Apennines (see Butler et al., 2004), but by the late-middle Pliocene, shortening was replaced by extension (e.g. Malinverno and Ryan, 1986; Mostardini and Merlini, 1986; Patacca et al., 1990; Cavinato and De Celles, 1999). Processes relating to today's extension are attributed to either isostatic rebound associated with detached lithosphere (Westaway, 1993), ongoing subcrustal processes involving mantle convective flow that affects surficial structures (D'Agostino et al., 2001) or to subducted slab retreat processes (Malinverno and Ryan, 1986; Royden et al., 1987; Doglioni et al., 1996; Cavinato and De Celles, 1999). The southern Apennines are characterised by heat-flows as high as 40–80 mW/m^2, the presence of active volcanoes (Vesuvius and Vulture), CO_2 emission sites (Mefite, Monticchio, Maschito and Contural), >20 °C hot-springs (S. Teodori and Contursi), and ^{3}He/^{4}He ratios of >1.5, indicating a relatively major mantle contribution to heat-flow (see Minissale, 2004 for details). In contrast, heat-flow in the central Apennines is only as high as 30–40 mW/m^2, and there are no major active volcanoes, CO_2 emission sites or >20 °C hot-springs, and mantle contributions to heat-flow are lower with ^{3}He/^{4}He ratios of >0.2 to <0.4. Despite this, the central and southern Apennines share similar P-wave velocity structures from tomography, and mantle anisotropy orientations from shear-wave splitting studies at 150 km depth, and free-air gravity values (D'Agostino et al., 2001; Margheriti et al., 2003).

Present day extension in the Apennines occurs across active normal faults that mostly strike parallel to the mountain chain (Anderson and Jackson, 1987; Cinque et al., 2000). The timing of initiation of extension in the southern Apennines probably occurred at around 1.8–3.0 Ma because in places Mid-Upper Pliocene sediments infill the hangingwall basins to the faults (Bartole et al., 1984; Westaway and Jackson, 1987; Westaway, 1987; Patacca et al., 1990; Knott and Turco, 1991; Oldow et al., 1993; Ferranti et al., 1996; Ascione and Romano, 1999; Ascione et al., 2003; Barchi et al., in press). Extension is associated with Ms 5.5–7.0 surface faulting earthquakes (e.g. Westaway and Jackson, 1987; Bernard and Zollo, 1989; Boschi et al., 1995; Michetti et al., 1997; Selvaggi et al., 1997; Michetti et al., 2000; Porfido et al., 2002), such as the 1980 Irpinia earthquake (Ms 6.9–7.0; c. 3000 deaths). These events record normal faulting and a NE–SW extension, consistent with borehole break-out and fault-slip data (Anderson and Jackson, 1987; Amato et al., 1995; Hippolyte et al., 1995; Amato and Montone, 1997; Selvaggi et al., 1997). Michetti et al. (1997) (see also Cinti et al., 1997), revealed through trenching investigations that the most recent surface faulting event on the Pollino fault (Fig. 2b), occurred between the XIII and XV century A.D., but is not reported in the historical catalogue, implying that the historical record is incomplete for a period longer than 600–700 years. A number of other trench site investigations also provide invaluable information on the Holocene palaeoearthquakes and deformation rates in the region (e.g. D'Addezio et al., 1991; Pantosti et al., 1993; Vittori et al., 1995).

3. Geomorphological setting

Geomorphological offsets across active normal fault scarps displacing slopes formed during the last glacial maximum (c. 18 ka) allow assessment of the throw rates across the active faults in the Apennines. Roberts and Michetti (2004) and Papanikolaou et al. (2005) measured the vertical offsets across fault scarps in the central Apennines to reveal rates of throw across the faults since the last glacial maximum with the timing constrained via tephrachronology and radiocarbon ages for colluvial deposits around the faults. Also, ^{36}Cl exposure dating of a fault plane associated with a scarp has supported the results of these workers, revealing that the scarps are indeed post-glacial (Palumbo et al., 2004). These workers found that the Magnola fault in the central Apennines has accumulated c. 12 m of slip in c. 12 kyrs through repetition of metre-sized slip events, implying a slip rate of about 1 mm/yr. This paper builds on the above and presents data on the vertical offsets across post-last-glacial-maximum faults scarps in the southern Apennines.

Several mountains in the southern Apennines show traces of former glaciations. All the glacial remains (moraines, till deposits, cirques) belong to the last glacial maximum between 21–18 ka, when the permanent snow line reached its lowest

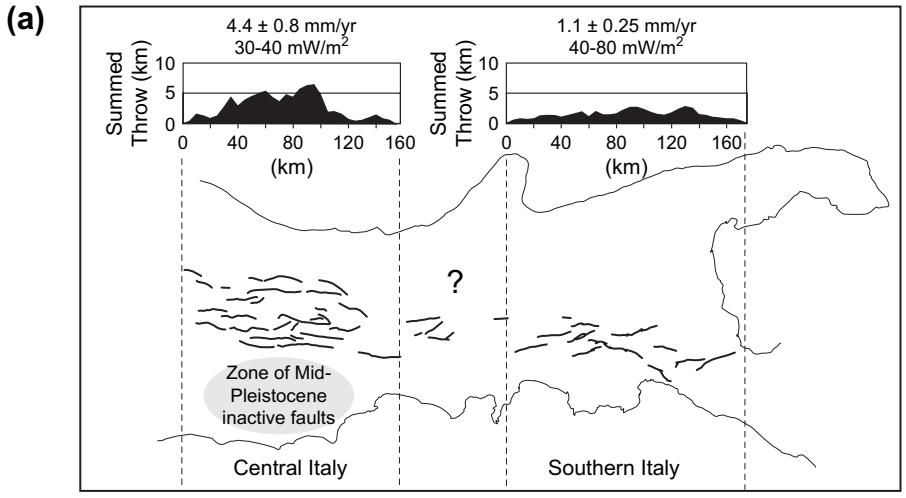
(a)
4.4 ± 0.8 mm/yr
30-40 mW/m2
1.1 ± 0.25 mm/yr
40-80 mW/m2
Summed Throw (km)
10
5
0
0 40 80 120 160
(km)
?
Zone of Mid-Pleistocene inactive faults
Central Italy
Southern Italy

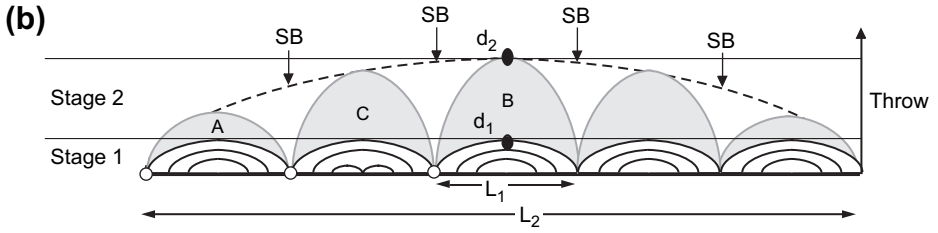
(b)
SB
SB
SB
SB
d2
d1
A
B
C
Stage 2
Stage 1
Throw
L1
L2

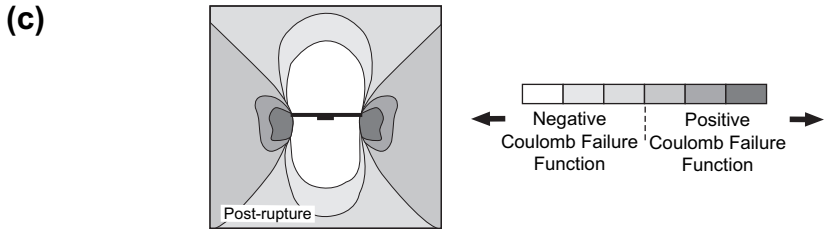
(c)
Post-rupture
Negative Coulomb Failure Function
Positive Coulomb Failure Function

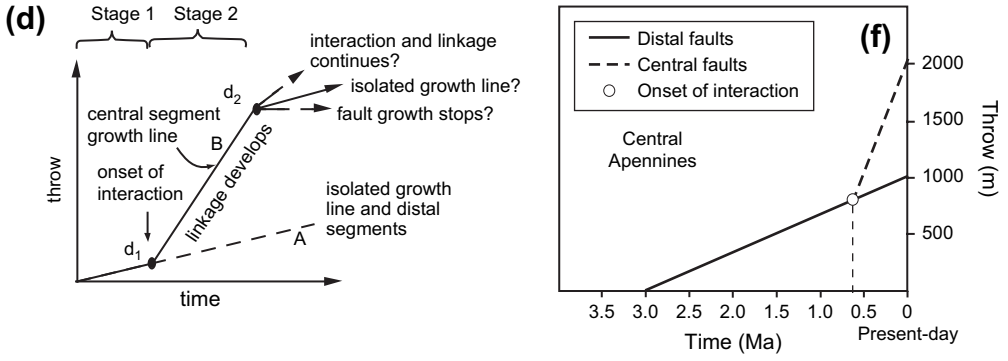
(d)
Stage 1
Stage 2
interaction and linkage continues?
isolated growth line?
fault growth stops?
central segment growth line
onset of interaction
linkage develops
isolated growth line and distal segments
throw
time
(f)
Distal faults
Central faults
Onset of interaction
Central Apennines
Throw (m)
Time (Ma)
Present-day

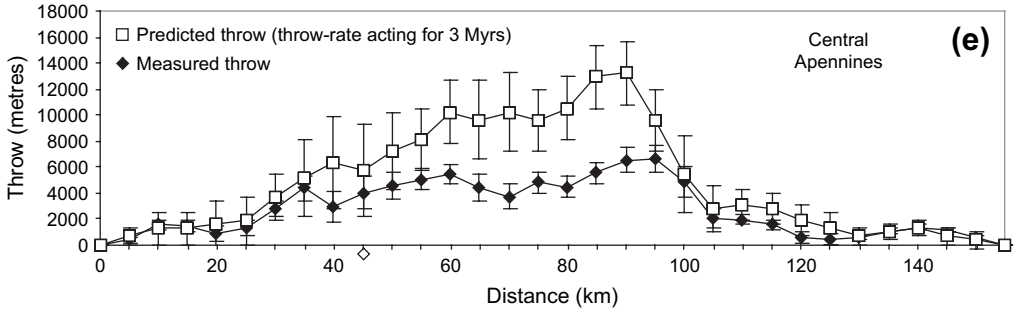
(e)
Predicted throw (throw-rate acting for 3 Myrs)
Measured throw
Central Apennines
Throw (metres)
Distance (km)

limit at about 1600–1750 m (Palmentola et al., 1990). Areas not covered by ice experienced periglacial conditions with vigorous freeze-thaw action, a sparse vegetation cover and high erosion and deposition rates. Scarps formed by ongoing active normal faulting were rapidly eroded and even buried by deposition of colluvial deposits because sedimentation and erosion rates exceeded fault throw rates. When the climate changed the slopes were preserved due to slope stabilisation related to re-establishment of temperate vegetation (e.g. Allen et al., 1999). It can be shown using tephrachronology that the last glacial maximum slopes are covered in only a few centimetres of Holocene deposits (e.g. Giraudi, 1995). Thus, scarps record the offset that has accumulated since the last glacial maximum at c. 18 ka. In this paper we present a detailed survey of the spatial variations in offsets across scarps, which we use to assess the spatial variation in throw rates across the faults averaged over 18 kyrs (Figs. 3–8). We assume the scarps date from 18 ka to minimise extension rates, although they could be as young as 12 ka (Palumbo et al., 2004).

4. Methodology

4.1. Fault map traces

The traces of all major active normal faults in the southern Apennines were identified from published geological maps and checked in the field; in places they were re-mapped using 1:100,000 topographic maps and a hand-held GPS (Fig. 2b). Determining the fault lengths is a difficult task because the faults appear to be segmented at a length scale of c. 5–15 km with small-scale en echelon fault overlaps (transfer zones or relay ramps) separating different fault segments. Additionally, some of the faults have very subtle geomorphic expressions where they enter rock types such as flysch or foredeep deposits close to fault tips. Following the methods of Roberts and Michetti (2004) who studied the central Apennines, we collected throw, throw-rate and kinematic information to help us verify fault lengths as described below.

4.2. Throw profiles

We constructed throw profiles by drawing serial cross-sections across each major active fault, using published 1:100,000 topographic and geological maps (Servizio Geologico D'Italia, 1969a,b, 1970a,b,c,d, 1971; CNR, 1990; Corrado et al., 2002) (Fig. 3), backed up by our field observations. An attempt was made to use the structural style visible on well-exposed faults to extrapolate above and below ground level during cross-section construction (see Roberts and Michetti, 2004). Errors on throws are variable and were quantified separately for every cross section. In most cases, errors represent 20–25% of the total finite throw values, which is sufficient for our purposes. Throw-distance profiles were constructed for each fault and our preliminary estimation of the fault tip locations was guided by a search for places where throws decrease to zero.

4.3. Fault slip directions

Striations, corrugations and fault plane orientations were measured at a number of localities along each fault in order to constrain the kinematics of the faulting and hence fault lengths (Figs. 6 and 7). Study of normal faults has shown that slip directions can help define fault lengths because they vary with throw and distance, converging towards the fault hangingwalls (Roberts, 1996; Michetti et al., 2000; Roberts and Ganas, 2000); fault lengths should therefore be reflected in the length-scale of the converging patterns of fault slip. We measured the strike and dip of faults and the plunge and plunge directions of lineations on fault planes close to the ends and centres of the normal faults indicated by the throw and fault trace analysis described above. We measured both the main fault planes (including variations due to the corrugated nature of the planes) and smaller minor fault surfaces in both the hangingwall and footwall where available. These 920 measurements were made at 47 localities. Localities were small (<c. 400 m^2) compared to the lengths of the faults (20–40 km). Mean values for the slip direction were calculated for each site using Fisher statistics in standard stereographic projection computer packages (Fig. 4). The errors on the mean values for each site are variable, but the mean error is $\pm 13.8^\circ$ at the 99% confidence level, a value that is much smaller than the observed variation (c. 145°).

4.4. Deformation rates

Deformation rates in the southern Apennines have been derived from published palaeoseismological results and new

Fig. 1. (a) Location map for the southern and central Apennines, Italy. Active faults shown offset Holocene sediments or landforms. Profiles show throws of pre-rift strata summed across strike for the active faults. Note the zone of faults that became inactive in the Mid-Pleistocene in the central Apennines; throws for these faults are not included in the profile. The summed throw profiles show that extension occurs in two distinct patches along the strike of the Apennines, and we use the lengths of these patches to define the lengths of the fault systems in the central and southern Apennines. Question mark indicates where throw data are unavailable. Values show extension rates (from Roberts and Michetti, 2004 and this study), and heatflow (from Minissale, 2004). (b) Model of how throw-distance profiles develop. Faults grow via lateral propagation and linkage/interaction in Stage 1. In Stage 2, faults interact across over longer distances via their stress fields in the manner shown in (c), and central faults develop enhanced slip rates as in (d). The overall displacement profile at the end of Stage 2 ($d_2 = \gamma L_2$) has the same throw/length ratio as the original shorter faults at the end of Stage 1 ($d_1 = \gamma L_1$). (c) Change in the Coulomb failure function following rupture of a normal fault in an earthquake. Optimally oriented faults in the zones of positive change are brought closer to failure whilst those in the zones of negative change have the time to failure increased. (d) Throw–time plots for central and distal faults in (b). (e) Detailed plot of cumulative throw summed across strike against distance along the strike of the fault system in the central Apennines. Also shown are throws that would develop if throw rates measured from the central Apennines were allowed to run for 3 Myrs, which is the time of fault initiation (Roberts and Michetti, 2004). The predicted throws exceed those measured in the centre of the fault system, consistent with the throw back-stripping shown in (f), and the idea that elastic interaction between faults causes increases in throw-rate on central faults (Cowie and Roberts, 2001). (f) Example of a throw–time plot from the central Apennines.

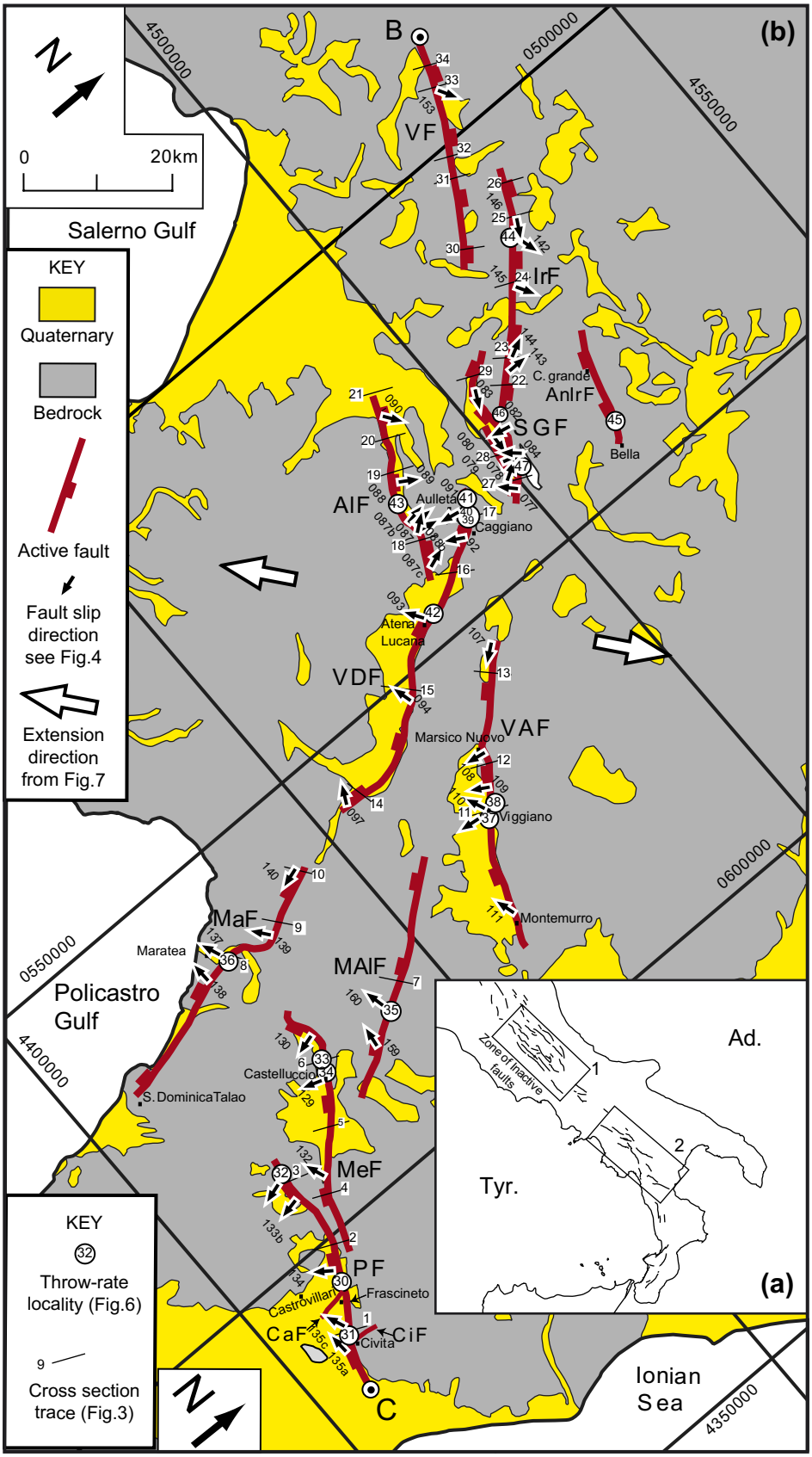

Fig. 2. (a) Location map showing the positions of the fault systems in the central and southern Apennines referred to in this paper. Tyr. is the Tyrrhenian Sea; Ad. is the Adriatic Sea. (b) Fault map with a UTM grid for the southern Apennines, located in (a). Arrows show fault slip directions from Fig. 4. VF, Volturara Fault; IrF, Irpinia Fault; AnIrF, Antithetic Irpinia Fault; SGF, San Gregorio Fault; AlF, Alburni Fault; VDF, Vallo di Diano Fault; VAF, Val d'Agri Fault; MaF, Maratea Fault; MAlF, Monte Alpi Fault; MeF, Mercure Fault; PF, Pollino Fault; CiF, Civita Fault; CaF, Castrovillari Fault. B–C: total length of the fault array.

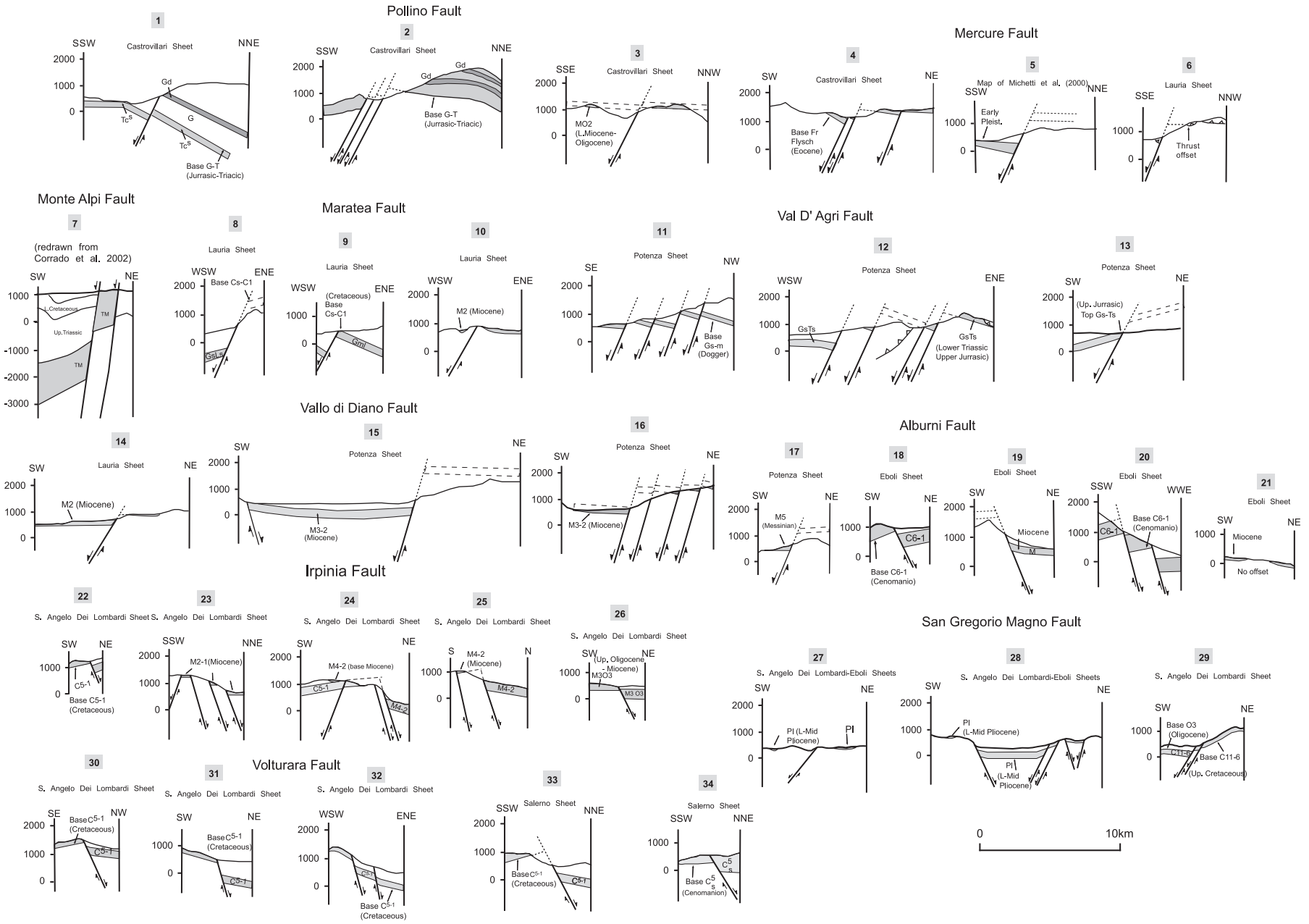

Fig. 3. Representative cross-sections across the faults in the southern Apennines from which throws across the faults were derived. Stratigraphic names are from the geological maps cited in the text. Cross-sections are located in Fig. 2.

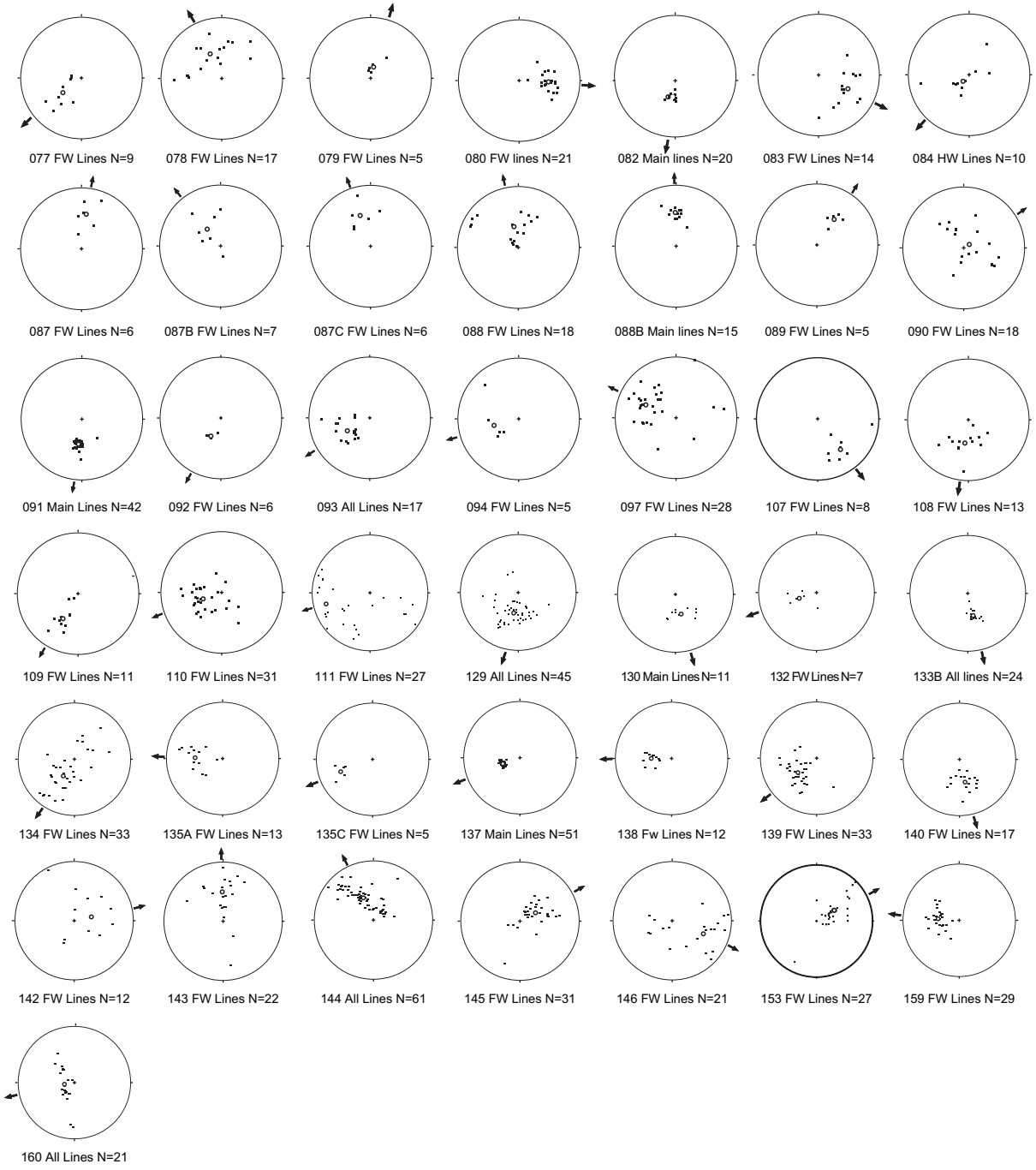

Fig. 4. Lower hemisphere stereographic projections of striations and corrugations on fault planes for localities shown on Fig. 2. Filled squares are individual measurements; open circles are the mean vectors calculated using Fisher statistics; black arrows are the azimuth of the mean vectors, which are also shown on Fig. 2. ''Main Lines'' means data were collected solely from the main fault plain separating syn-rift hangingwall rocks from pre-rift footwall rocks. ''FW Lines'' means data were collected from the footwall fault array within 10 m across strike of the main fault plane. ''All Lines'' means both data from the main fault plane and the footwall fault array are plotted on the same stereographic projection.

geomorphic observations of displaced 18 ka sediments and landforms (see Section 3). Quantitative data were extracted from topographic profiles measured perpendicular to the trace of fault scarps where the vertical offset of the 18 ka surfaces corresponds to the total throw in that time (Figs. 5 and 6) (see Papanikolaou, 2003 for more detailed scarp profile data). Care was taken to measure scarp profiles away from human disturbance, or post-18 ka erosion and sedimentation. Where scarps were inaccessible due to steep slopes, throw values were estimated in the field and then re-examined in the laboratory after examining photos with clear objects for scale. All the scarp profiles were constructed through chain surveying techniques using a ruler (1 m) and a clinometer. Errors on individual slope measurements were $<5^{\circ}$, whilst errors in the chain surveying would show a Gaussian distribution about the actual values and cancel out; this was confirmed

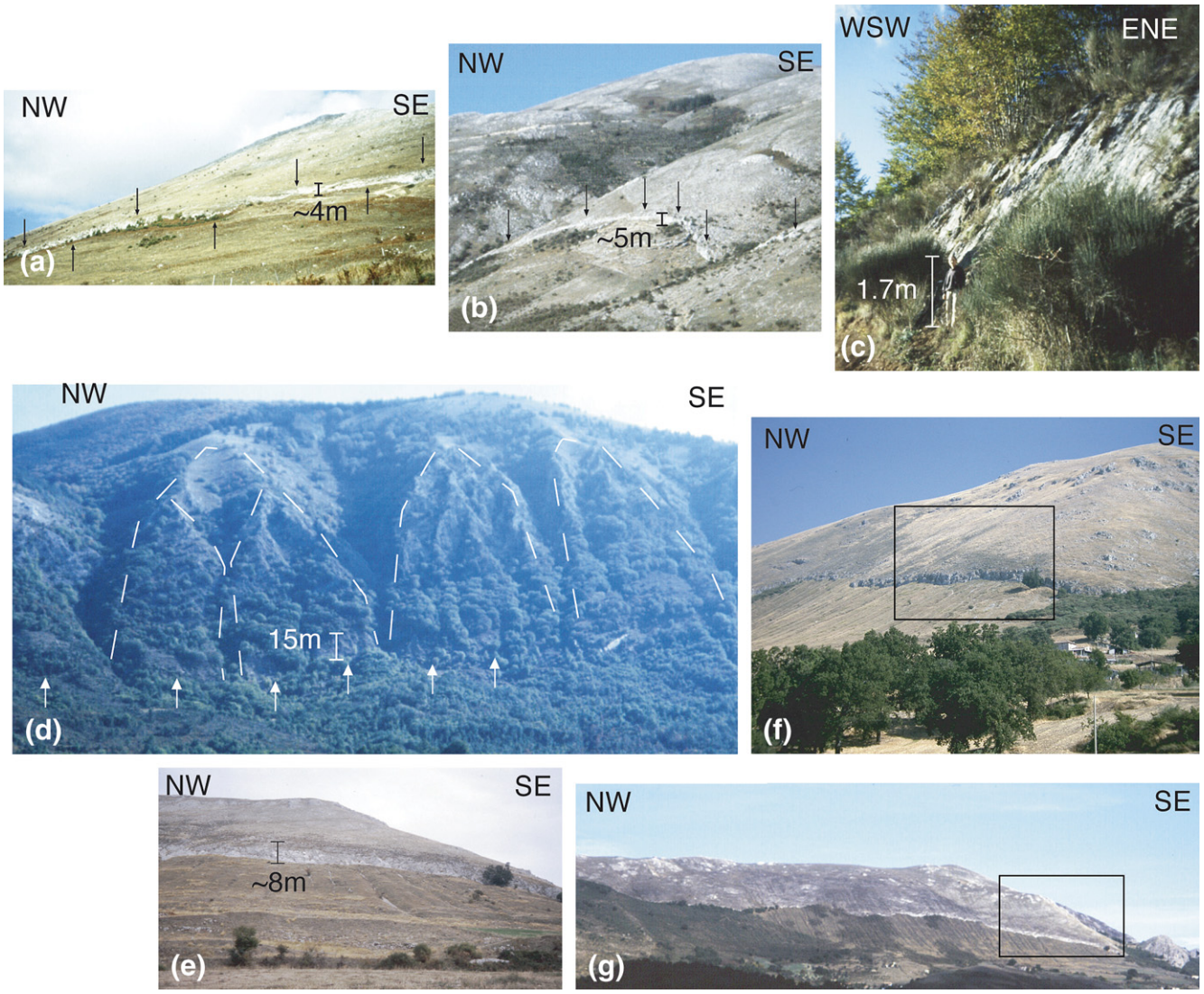

Fig. 5. Representative photographs of post-glacial fault scarps in the southern Apennines. (a) c. 4 m of post-glacial throw across the Antithetic Irpinia Fault. (b) c. 5 metres post-glacial throw across the San Gregorio Fault. (c) 4.0–4.5 m of post-glacial throw across the Pollino Fault. (d) c. 15 m of post-glacial throw across the Val d'Agri Fault. Dashed lines outline triangular facets. (e) c. 8 m of post-glacial throw across the Val di Diano Fault, located in (f) and (g); (f,g) alternative views of the post-glacial scarp on the Val di Diano Fault. (e) and (g) are looking towards the east; (f) is looking towards the north.

where elevations were checked with a barometric altimeter with an accuracy of ±1 m. Profiles were reconstructed and interpreted in a graphics package and the following features were interpreted following established methods (Avouac, 1993; Yeats et al., 1997); the upper slope, a degraded scarp, a free face, a colluvial wedge and a lower slope. The post 18 ka throw is defined as the vertical distance measured between the intersections of projections of the fault plane, and the upper and the lower slopes.

We estimate that the total error on the post-18 ka throw is <c. 20% (Fig. 8), so errors in throw rates across individual scarps are everywhere <0.2 mm/yr where we have a scarp profile. Where we estimated throws across scarps we show higher errors determined in the field. In the southern Apennines, all the throws that have been estimated visually exhibit low throw rates (<0.7 mm/yr), so an error of ±3.6 m (±0.2 mm/yr) is estimated for scarps of 5.4 m to 10.8 m high (0.3–0.6 mm/yr) and an error of ±1.8 m (±0.1 mm/yr) is used for scarps less than 5.4 m high (<0.3 mm/yr).

5. Results

5.1. The lengths and positions of major normal faults

We have identified 11 major active normal faults which exhibit post 18 ka surface faulting. Throws across these faults vary over distances of about, 20–45 km, showing clear maxima and minima (Fig. 8). The minima indicate the lateral fault tips. This interpretation is supported by fault-slip direction data which show converging patterns of slip (Fig. 2b). The converging slip directions support the throw patterns because they indicate along-strike stretching of the ground that is consistent with the throw variations. Measured throw rates also vary over distances of about, 20–45 km, showing maxima

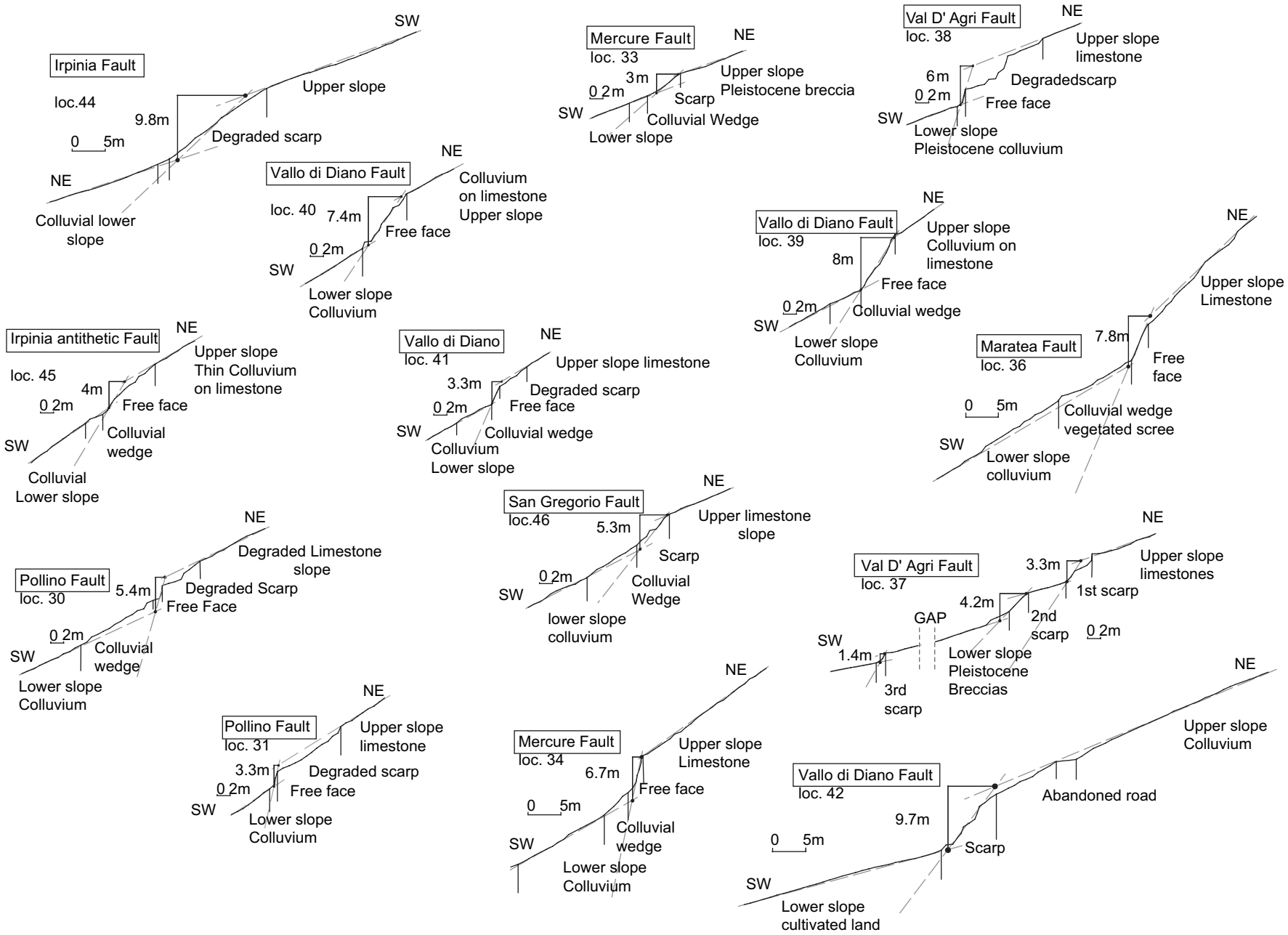

Fig. 6. Profiles across post-glacial scarps in the southern Apennines from which throw rates have been derived. Profiles are located in Fig. 2. Longer profiles with photographs are presented in Papanikolaou (2003).

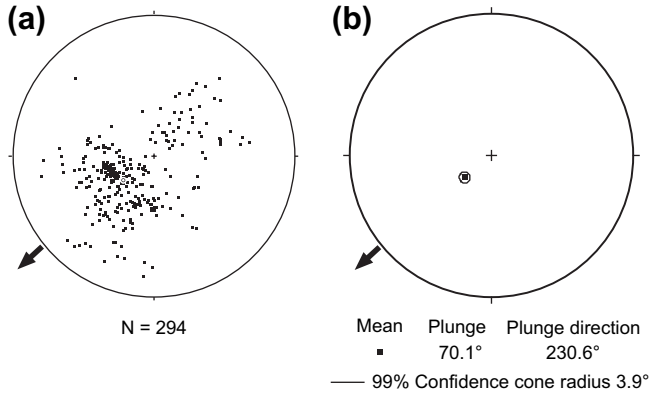

Fig. 7. Lower hemisphere stereographic projections of striations and corrugations on fault planes from the centres of the faults in southern Italy. Data are an extract of those in Fig. 4. (a) Small black squares are individual measurements. Small open circle is the mean vector. (b) Mean vector and 99% confidence cone.

and minima that coincide geographically with the throw maxima and minima, and places where large (c. 90° or more) variations in slip direction exist between neighbouring major faults (Fig. 8). Thus, the throw rates are also consistent with our interpretation of fault lengths. We stress that the slip direction, throw and throw-rate values are derived from independent data sources, and the fact that they agree suggests that our interpretation of fault lengths is robust. Table 1 gives a full account of our data and highlights where we agree or disagree with throw and throw-rate measurements of other workers; our data mostly agree with other workers. Although the faults appear to be characterised by symmetrical throw and throw-rate profiles, this may be due to the low spatial resolution we have achieved close to fault tips. We also note that faults appear not to be linked, as relay zones between faults do not appear to contain significant fault offsets. This structural style is similar to that recorded in the central Apennines (Piccardi et al., 1999; Roberts and Michetti, 2004).

5.2. Regional kinematics

We have compiled fault slip direction data from the centres of the faults to calculate the mean fault slip direction and hence the kinematics for the active fault array (Fig. 7). We have not used data from localities positioned away from the interpreted centres of the faults because they will be controlled by strains produced by along strike stretching of hangingwall and footwall surfaces. The mean fault slip direction for the active fault array is 70.1° plunge towards 230.6 ± 3.9° at the 99% confidence level ($N = 294$) (Fig. 7). This is consistent with the NE–SW σ^3 orientation of the active stress field (Amato et al., 1995; Amato and Montone, 1997; Selvaggi et al., 1997). This direction is about 90° to the fault strikes in the region (NW-SE) so the faulting is almost pure dip slip (Fig. 2b). These values are very similar to those in the central Apennines measured by Roberts and Michetti (2004) (62° plunge towards 222 ± 4° at the 99% confidence level; $N = 189$), reinforcing the notion that the central and southern Apennines have experienced the same tectonic boundary conditions.

The conclusion that the southern Apennines contains faults with overall dip–slip kinematics contrasts with the studies of other workers who suggest a NNE–SSW extension or a regional oblique extension involving the presence of strike slip faults (Hippolyte et al., 1994; Cello et al., 1997; Monaco et al., 1998; Van Dijk et al., 2000). For example, Hippolyte et al. (1994) suggested that slip data towards the northwestern end of the Vallo di Diano fault, indicated a NNE–SSW regional extension. However, we suggest that the above measurement, derived from the northwestern end of the fault, does not indicate a regional extension direction because slip vectors close to the tip of the fault converge towards its hangingwall to accommodate stretching of the ground surface along strike the fault. Slip vectors derived from the centre of the Vallo di Diano fault on a post-glacial fault scarp display almost pure dip–slip motion, indicating NE–SW extension (Figs. 2b and 4). Thus, although local oblique or strike-slip motions occur near fault tips, as is common in other extensional areas (Roberts, 1996; Roberts and Ganas, 2000; Roberts and Michetti, 2004), the extension in the southern Apennines is predominantly NE–SW dip–slip.

The conclusion that the motions are predominantly dip–slip implies that differential rotations about vertical axes for different fault blocks will be minimal during extension. This is consistent with palaeomagnetic data from the Apennines that show no significant post middle-Pleistocene rotations about vertical axes (Speranza et al., 1998); measured rotations of small magnitude for Pliocene rocks are probably due to the last phase of compression in this sector of the Apennines (Gattacceca and Speranza, 2002). Thus, in the absence of significant rotations about vertical axes during normal fault activity, the heave directions at the centres of the faults can be considered to be the extension direction.

5.3. Cumulative throw and throw-rate diagram

In order to study how cumulative throw and throw-rate values vary along the strike of the fault system, throw and throw-rate profiles for individual faults were constructed (Fig. 8) and then summed across strike to produce cumulative throw and throw-rate profiles (Figs. 1 and 9). Values were summed along 36 NW–SE transects across the faults located every 5 km along strike.

The cumulative throw and throw-rate profiles show a number of local maxima and minima. However, overall the summed profiles resemble that for a single fault in that the maxima occur close to the centres of the profiles, consistent with interaction between these crustal scale faults. The summed profiles show maxima of 3100 ± 700 m and 1.1 ± 0.25 mm/yr, respectively. Throws and throw rates decrease to zero at the ends of the fault system. This is not because we have simply stopped collecting data. In these locations, it is possible to travel across the Apennines without crossing an active normal fault that is known to us. For example, to the immediate southeast of the Pollino fault, no other major active faults are known

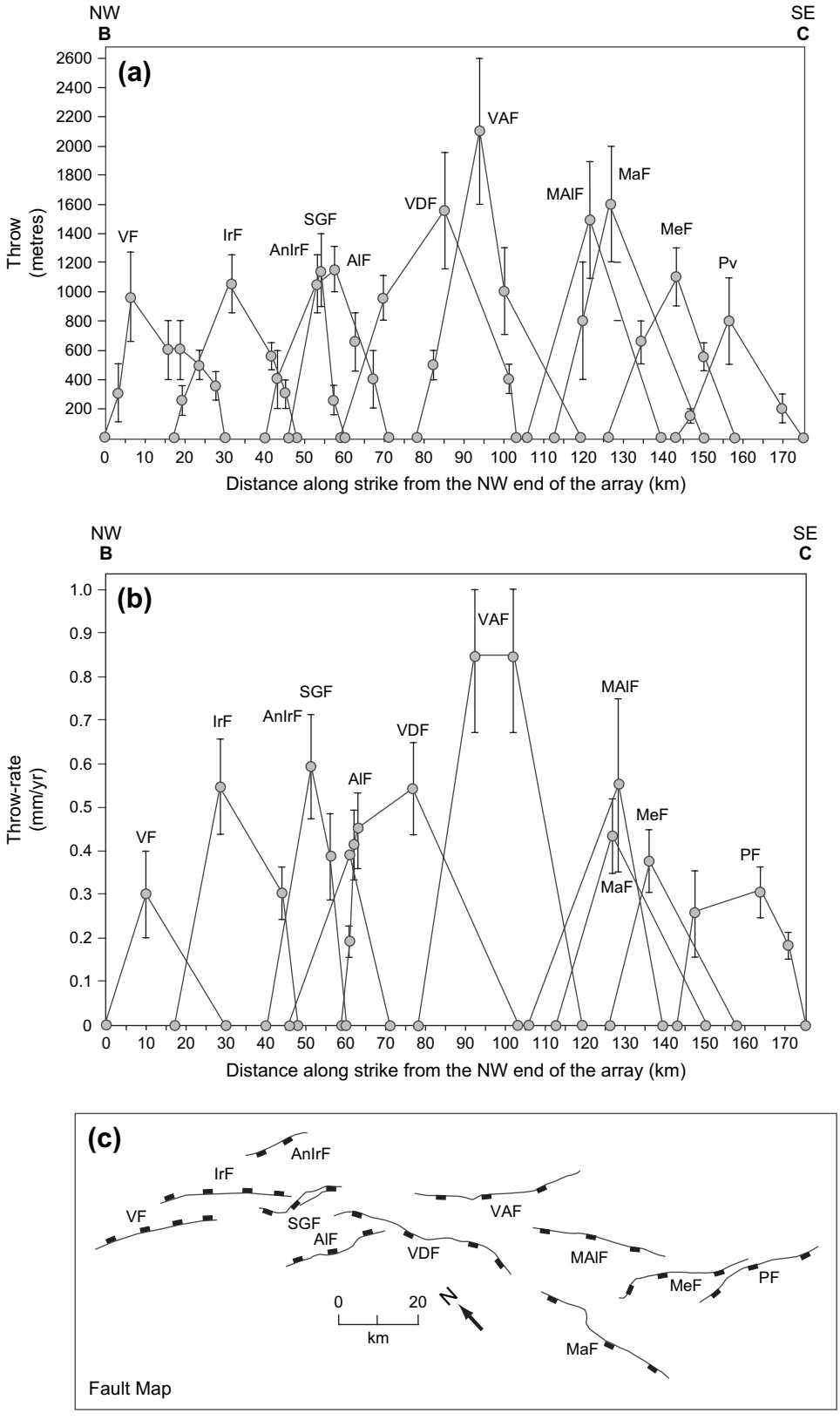

Fig. 8. (a) Throw–distance plots for individual faults in the southern Apennines. (b) Throw-rate–distance plots for individual faults in the southern Apennines. (c) Fault map drawn at the same scale. Fault names are as for Fig. 2.

to exist. The nearest reported active faults are located about 40 km towards the southwest of the Pollino fault, in the Crati valley and form part of the N–S trending Calabrian fault system (Tortorici et al., 1995). Similarly, northwards from the Volturara fault, it is possible to draw a straight NE–SW oriented transect, without crossing a known active fault. The nearest known active fault is located a few tens of kilometres northwest from the Volturara fault and probably hosted the 1962 earthquake sequence (Ms = 6.0, Westaway, 1987), whereas major surface faulting normal faults are located further northwards from the 1962 earthquake sequence in the area of Benevento related to the 1688 historical event (Di Bucci et al., 2006) and in the Matese massif (Di Bucci et al., 2005). Overall, it appears that the extension on major normal faults dies out northeast of the Volturara fault and southeast of the Pollino fault, before reaching any other active faults. Extension in the southern Apennines, occurs as discrete patches, like that in the central Apennines (Fig. 1).

5.4. Extension rates

Large seismogenic normal faults are approximately planar in cross section and the majority have dips in the range between 30° and 60° (Jackson and White, 1989). Thus, we have converted the summed throw rates (Fig. 9) into heave-rates, assuming planar fault geometries and a 45° fault dip. As we have already concluded above (Section 5.2) that overall the faults accommodate almost pure dip–slip motion with very low rates of rotation about vertical axes, we can assume that the extension direction is the same as the heave direction, that is, $230.6 \pm 3.9°$. Thus, a maximum extension rate of 1.1 ± 0.25 mm/yr in a direction of 231–051° is implied. The curve connecting points on Fig. 9b can be considered to show the spatial variation in extension rates. This assumes pure dip–slip at all points along the faults, and does not take into account the oblique-slip we have measured close to fault tips; if taken into account, this would decrease the overall extension rate value by up to about 20%, where values are summed in the vicinity of fault tips. Also, our data on fault dips, extracted from fault planes exposed at the surface show steeper dips (50–65°) than we have assumed; clearly this would imply an even lower extension rate. However, we do not know exactly how surface fault dips relate to those at depth. The focal mechanisms for the 1980 Irpinia earthquake sequence showed 60° dips for the main rupture, and 70° dips for the antithetic rupture (e.g. Westaway and Jackson, 1987; Pantosti and Valensise, 1990; Cocco and Pacor, 1993). On the other hand, seismic reflection profiles suggest an approximately 50° dip for the Val D'Agri fault and a 45° dip for the Vallo di Diano fault (Noguera and Rea, 2000; Barchi et al., in press). As a result, we believe that a 45° fault dip value is probably a lower bound for the normal faults in the southern Apennines, thus providing a maximum value for the extension rate. If we use a higher fault dip value such as 50°, a lower extension rate of 0.92 ± 0.21 mm/yr is implied, with a rate of 0.64 ± 0.14 mm/yr for a 60° dip. The rates we suggest are at the lower end of the range suggested by palaeoseismology, seismic moment summations and geodesy (1–6 mm/yr; Westaway, 1992; Pantosti et al., 1993; Anzidei et al., 2001; Hunstad et al., 2003; Nocquet and Calais, 2004). We note that if extension rates as high as 6 mm/yr were concentrated on faults we have mapped, and a 45° fault dip is assumed, deformation for 18 kyrs would imply a summed scarp height across all the faults of 108 m (72 m if scarps date from 12 ka; Palumbo et al., 2004). We have measured a maximum summed scarp height of only c. 20 m (Fig. 9b). We find it inconceivable that we, and other workers, have missed 52–88 m of throw across post 18 ka scarps. Explanation of this discrepancy will have to await studies of the relationship between strains associated with surface faulting and those measured during interseismic strain accumulation (Papanikolaou et al., 2005).

6. Analysis of throw, throw-rate and fault-length relationships

6.1. Spatial variation in throw/length ratios

The faults described above have lengths in the range of, 20–45 km and maximum throws between 700 and 2100 m (Table 1). Their throw/length ratios are 0.025–0.058 (Fig. 10), similar to values for faults in the central Apennines (0.035–0.083; Roberts and Michetti, 2004). These values are towards the higher end range of equivalent displacement/length ratios recorded from worldwide databases (0.001–0.1; Schlische et al., 1996).

Central faults tend to have higher throw/length ratios than distal faults in the southern Apennines (Fig. 11a). The overall array has a length of 175 km and cumulative throw summed across strike of 3100 ± 700 m, implying a throw/length ratio in the range 0.014–0.022 (Fig. 10); the equivalent value for the central Apennines is 0.014 (Roberts and Michetti, 2004). Thus, like in the central Apennines, the overall array is under-displaced relative to individual faults within the array, as expected from Fig. 1c. This may explain why the central faults have higher throw rates than distal faults; the central faults may be growing more rapidly, achieving higher individual throw/length ratios, in order to achieve an overall throw/length ratio concomitant with its length and geological setting (Cowie and Roberts, 2001). This implies interaction between these crustal-scale faults, in the manner described in Fig. 1.

6.2. Spatial variation in finite throws

Throws along individual faults decrease from maxima close to their centres to minima at fault tips (Figs. 8 and 12a). Quantitative analysis shows a relatively strong positive correlation ($R^2 = 0.63$) between maximum finite throw values and distance along strike from the nearest end of the overall fault array (Fig. 11b; see also Fig. 12d for an indirect measure of the throw maxima). This is also true of gradients in throw (Fig. 12a,c). Thus, faults with the

Table 1
Lengths, positions, finite throw and throw-rate data of major active faults

Fault name	Length (km)	Max. throw (m)	Error in m	Locality number (Fig. 2)	*X* UTM	*Y* UTM	Post-18 ka throw (m)	Error in m	Throw-rate (mm/yr)	Data source	Notes
Pollino	32	800	300		0605483	4412366	6		0.33-0.4	S.P.,T.	Bedrock scarp and trench site data from Vittori et al., 1995; Michetti et al., 1997.
				30	0605223	4412845	5.4	1.1	0.3	S.P.	Bedrock scarp.
				31	0611287	4409150	3.5	0.7	0.19	S.P.	Bedrock scarp.
				32	0588419	4416598	4-4.5	1.8	0.22-0.25	E.E	Bedrock scarp, lower slope disturbed by cultivation.
									0.2-0.5	S.P.	Long-term throw-rate data from Cinti et al., 1997, 2002 (Castrovillari fault). We consider the Castrovillari fault to be a release fault along the Pollino fault due to the converging slip-patterns along the latter.
Mercure	32	1100	200	33	0581379	4430162	3	0.6	0.17	S.P.	Alluvial scarp in a chestnut wood forest close to triangular facets in the footwall.
				34	0582178	4429629	6.7	1.3	0.37	S.P.	Bedrock scarp on the continuation of the previous scarp, a few hundred meters towards the SE.
Monte Alpi	33	1500	400	35	0582017	4440880	9-10	3.6	0.55	E.E.	5–6 m polished fault surface plus 3–4 m of degraded scarp, along the steep limestone escarpment. Range front exhibits an oversteepened portion near its base. (see also Van Dijk et al., 2000). Finite throw value extracted from Corrado et al. (2002) cross-section based on seismic reflection and well logs.
Maratea	37	1600	400	36	0562700	4429519	7.8	1.6	0.43	S.P.	Bedrock scarp, a portion of the upper slope is exposed. Range front exhibits an oversteepened portion near its base.
							7-10			E.E.	Data from Hippolyte et al. (1994).
Val D' Agri	41	2100	500		0564879 0564853	4475800 4476092	15		0.83	E.E.	c. 15 m throw on post-glacial bedrock scarp on a SW dipping fault that offsets footwall streams at the base of triangular facets (see also Benedetti et al., 1998). Range front exhibits an oversteepened portion near its base. We also suggest following Benedetti et al., (1998), Collela et al., (2004) as well as Barchi et al., (in press) that this is the main fault. However, Maschio et al., (2005) suggest that the activity has now shifted to the NE dipping fault. An antithetic northeast dipping fault is located 4-5 km west from the main Val D'Agri fault. However, the low topographic relief associated with it, indicates that if it is active, it is expected to exhibit a low throw-rate value (<2–3 m postglacial throw: <0.2 mm/yr throw rate). Indeed, seismic reflection data show that this fault has a very small finite throw and joins with the main fault at a shallow depth (6 km) (Noguera and Rea, 2000; Barchi et al., in press). Maschio et al., (2005) estimate a throw rate of 0.25–35 mm/yr and a finite throw of 300 m for this fault that are on the threshold of observation.
				37	0571296	4468174	9	1.8	0.5	S.P.	Lower heavily degraded bedrock scarp.
				38	0570741	4469864	6	1.2	0.33	S.P.	Upper bedrock scarp.
							15	3	0.83	S.P.	Cumulative postglacial throw across bedrock scarps (Upper scarp loc. 37 + lower scarp loc. 38).
Vallo di Diano	45	1550	400	39	0538726	4491971	8	1.6	0.44	S.P.	Post glacial bedrock scarp showing throw variation along strike over short distances. Footwall shows little degradation and the hangingwall Pleistocene colluvium is covered by only 10–20 cm of organic-rich Holocene soil.

				40	0538539	4492238	7.3	1.5	0.41	S.P.	Postglacial throw diminishes towards the NW tip of the fault, from 8 m to 7.3 m and 3.3 m, 4 km, 3.5 km and 2 km away from the tip, respectively.
				41	0537182	4492810	3.3	0.7	0.18	S.P.	
				42	0545958	4479775	9.8	2	0.54	S.P.	Bedrock scarp, lower slope is disturbed by cultivation.
Alburni	25	1150	150	43	0532258	4485676	6-7	3.6	0.39	E.E	Degraded bedrock scarp is hidden by the vegetation, but free-face exists.
Irpinia	31	1050	200	44	0515232	4520580	9.8	2	0.54	S.P.	Scarp across colluvium in a chestnut wood forest. We suggest the fault continues across the Sele Valley due to the converging patterns of slip and the continuity of the throw profile. The fault has a subdued topographic expression as it crosses the Sele valley due to lithologies that have a low resistance to erosion relative to limestone. The converging pattern of slip explains the difference in extension directions implied by striated faults at outcrop and the 1980 focal mechanisms.
									0.25-0.35	T.	Trench site data from Pantosti et al., 1993.
Irpinia Antithetic	15			45	0542557	4514780	4	0.8	0.22	S.P.	Bedrock scarp near Bella. (see also Bernard and Zollo, 1989; Blumetti et al., 2003). The antithetic Irpinia fault is not considered as a major fault due to its short length ($\leq$15 km) and low throw-rate ($\sim$0.2 mm/yr) and thus it has been excluded from the calculations made later in this paper.
San Gregorio	20	1150	250	46	0532772	4502364	5.3	1.1	0.29	S.P.	Bedrock scarp on a SW dipping fault. We suggest this is the main fault as it displays converging slip directions that correlate with spatial variations in the scarp height. (see also Ascione et al., 2003; Cinque et al., 2000, who estimate a slip rate less than 0.5 mm/yr for this fault).
									0.3	T.	Trench site data from D'Addezio et al., 1991 on the NE dipping fault.
				47	0538239	4500441	1.5		0.08	E.E.	Postglacial throw diminishes towards Balvano village.
Volturara	30	950	300						$\leq$0.3	E.E.	No bedrock scarp observed, possibly covered by lake sediments. Activity indicated by the presence of two windgaps between the Village of Volturara and the village of S. Stefano.

Data source shows whether a trenching (T.) or scarp profile (S.P.) was constructed, or throws across scarps were estimated by eye (E.E.).

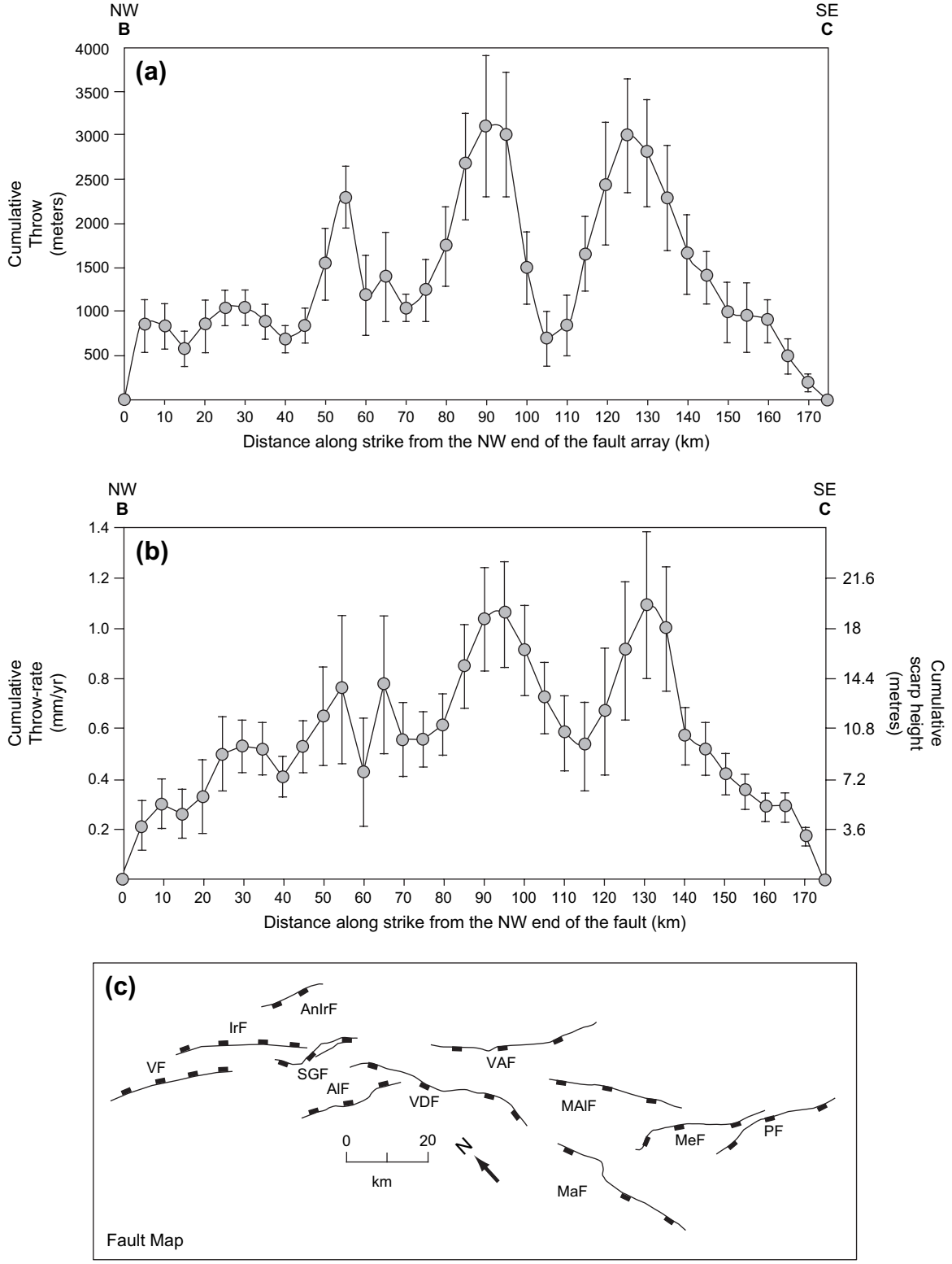

Fig. 9. (a) Cumulative throw–distance plot for the southern Apennines; a simplified version is shown in Fig. 1. (b) Cumulative throw-rate–distance plot for the southern Apennines. (c) Fault map drawn at the same scale. Data are summed from across-strike transects located every 5 km along the strike of the fault system. Fault names are as for Fig. 2.

greatest throws and steepest throw gradients are positioned in the centre of the array, again consistent with the idea of interaction between these crustal-scale faults (compare with Fig. 1c).

6.3. Spatial variation in throw rates

Centrally located faults exhibit higher throw rates compared to the distal faults (Fig. 11c; see also Fig. 12e for an

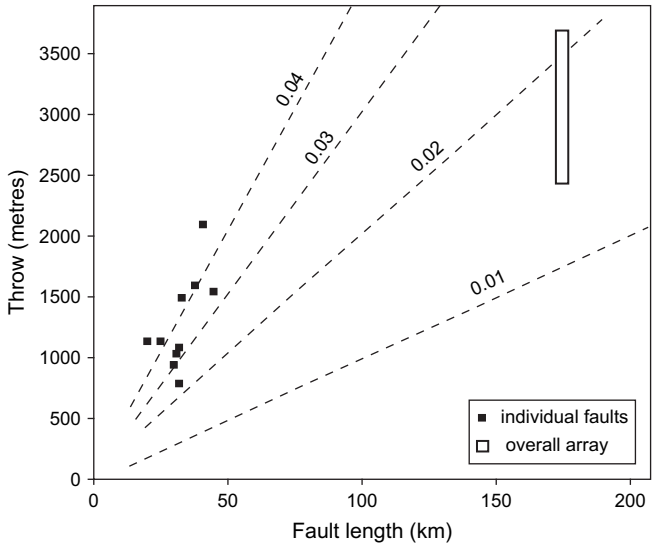

Fig. 10. Plot showing throw/length ratios for faults in the southern Apennines. The overall array is under-displaced relative to individual faults within the array.

indirect measure of the throw-rate maxima). Centrally located faults also exhibit higher throw-rate gradients compared to the distal faults (Fig. 12b,e). Again we suggest that the central faults may be growing more rapidly, achieving higher individual throw/length ratios, in order to achieve an overall throw/length ratio concomitant with the overall length of the array and its geological setting (Cowie and Roberts, 2001) (see Fig. 1c).

6.4. Interpretation

Our results suggest that individual faults are working together to produce cumulative throw and throw-rate profiles that resemble that expected for a single fault (Fig. 9). This clearly demonstrates that even though the faults are not physically linked by slip surfaces, these crustal-scale faults interact (Fig. 1d), and form a 175 km long soft-linked fault array.

However, the key question for this paper remains: when did the faults begin to interact and exhibit higher throw rates on central faults? The central Apennines began to show increased throw rates on central faults and overall profile readjustment late in the finite fault growth history (c. 75% of the elapsed time; Fig. 1g). This was recognised because the Fucino fault at the centre of the central Apennines fault array is slipping at 2 mm/yr averaged over 18 kyrs, but has only accumulated 2 km of throw, even though Upper Pliocene hangingwall stratigraphy that could be as old as 3.4 Ma, thickens into the fault (Cavinato et al., 2002). Also, if total throws are divided by throw rates, central faults appear to exhibit younger ages (Fig. 13a); this is not the case, however, as this is due to the fact that throw rates on central faults have increased relative to distal faults (compare with Fig. 1b). In the next section we carry out similar calculations for the southern Apennines to assess if throw rates varied through the faulting history.

7. Longevity of fault throw rates

We divide the throw maxima by the throw-rate maxima for each fault in the southern Apennines to see if throw rates since 18 ka are large compared to total throws for central faults compared to distal faults (Fig. 13b). In contrast to the central Apennines (Fig. 13a), data for the southern Apennines show that the above ratio shows little or no correlation with distance along the fault array (Fig. 13b). This implies that post 18 ka throw rates on central faults, although higher than those on distal faults (Fig. 11c), can explain the total throws, and are thus not inconsistent with stratigraphic data which imply initiation of extension at 1.8–3.0 Ma. Again in contrast to the central Apennines, if post 18 ka throw rates are allowed to run for 3.0 Ma, they produce throws that are comparable with those measured (compare Figs. 1e and 13c). Thus, for individual faults, throw-backstripping using post 18 ka throw rates implies fault initiation ages that lie within the range of uncertainty provided by stratigraphic data (1.8–3.0 Ma; Fig. 13d). These findings indicate that, within the resolution of our data, throw rates appear to have been constant from the time when faulting started in the southern Apennines. This is consistent with the findings of Nicol et al. (1997), Walsh et al. (2001, 2002), and Meyer et al. (2002), but different to results from the central Apennines and other faults systems (see Section 1).

8. Throw rates and throw–length relationships

Finally, we assess whether it is sensible to extrapolate throw rates averaged over 18 kyrs over the entire history of faulting. As throw rates must eventually produce total throws that conform to scaling relationships between throw and length, we use the method of Cowie and Roberts (2001) to see if this is true of the post 18 ka throw rates we have measured. We calculate throw-rate enhancement factors using the method presented by Cowie and Roberts (2001) (Table 2). This calculation predicts the throw rates that are need to eventually produce a throw/length ratio for the overall array that is the same as that for the distal faults in the array at the instant when fault interaction develops. The spatial variation in enhancement factors (E) for throw rates on faults in an interacting array which has a triangular throw profile can be calculated using the relationship $2R_i/L_i$, where L_i is the length of the i-th fault and R_i is the distance between the fault midpoint and the nearest tip of the overall array (Cowie and Roberts, 2001). Values from Table 1 were input into this equation to perform the calculation (Table 2). Fig. 14 shows that the predicted throw rates fall very close to, or within error of our measurements, lending confidence to our measurements of throw-rate. This confirms that the spatial variation in throw rates can produce a throw/length ratio for the overall array that is the same as that for the distal faults; the post 18 ka throw rates are likely to be representative of longer term throw rates, consistent with Section 7.

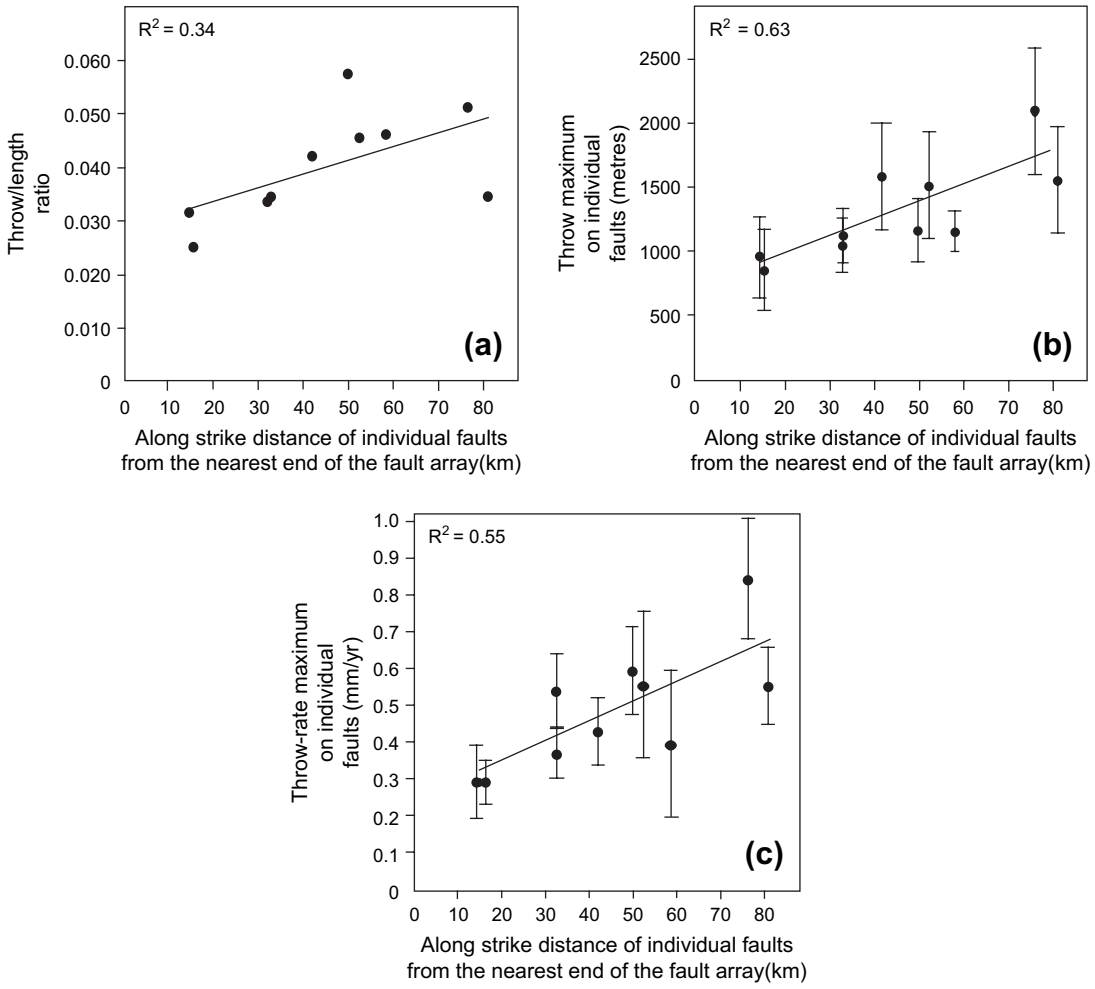

Fig. 11. Plots showing how throw/length ratios (a), maximum throws (b), and maximum throw rates (c) for individual faults vary along the strike of the overall fault system.

9. Discussion

We have presented evidence that the growth histories of two fault systems from the central and southern Apennines are very different. Throw rates increased by a factor of 6 late in the faulting history in the central Apennines, whereas we cannot resolve any temporal changes in throw rate in the southern Apennines. The two areas share the same tectonic boundary conditions and lithospheric structure, so that it is difficult to argue that they have experienced different loading histories and hence throw-rate histories.

The main differences between the two areas appear to be the higher heat-flow in the southern Apennines, and the geometric history of the fault systems. It is clear that extension in the central Apennines was associated with death of large basin-bounding faults in the Mid-Pleistocene synchronous with an increase in throw rates on faults that remained active (Section 1). If regional strain rates were constant, fault death may have caused an increase in throw-rate on faults that remained active (Roberts et al., 2002). As death of large basin-bounding faults is not evident in the southern Apennines, this may explain why we cannot resolve any increases in throw-rate. The initially localised geometry of the southern Apennines may have been due to the higher heat-flow, causing earlier onset of thermal/rheological perturbations and localised flow at depth (Cowie et al., 2005), but this needs further work.

However, we must add a cautionary note to our conclusion that throw rates in the southern Apennines appear to have remained constant through time. We are aware of how poorly the early history of faulting is resolved, as uncertainty on the initiation age for faulting (1.8–3.0 Ma) is at least 40% of the total duration of faulting. Also, we note that death of faults with offsets of less than a few hundred metres would not be resolved by existing mapping. An increase in throw rates could have occurred early in the faulting history, at a time when offsets across faults that ceased in activity were relatively small; this deformation would be difficult to resolve stratigraphically. Thus, the possibility exists that slip rates may have increased in the first few percent of the faulting history.

This uncertainty is not trivial because recognition of whether fault slip rates can indeed be constant from fault initiation is crucial to understanding what processes drive spatial variations in slip rates. We note that observations prove that faults located centrally within a fault systems slip more rapidly than distal

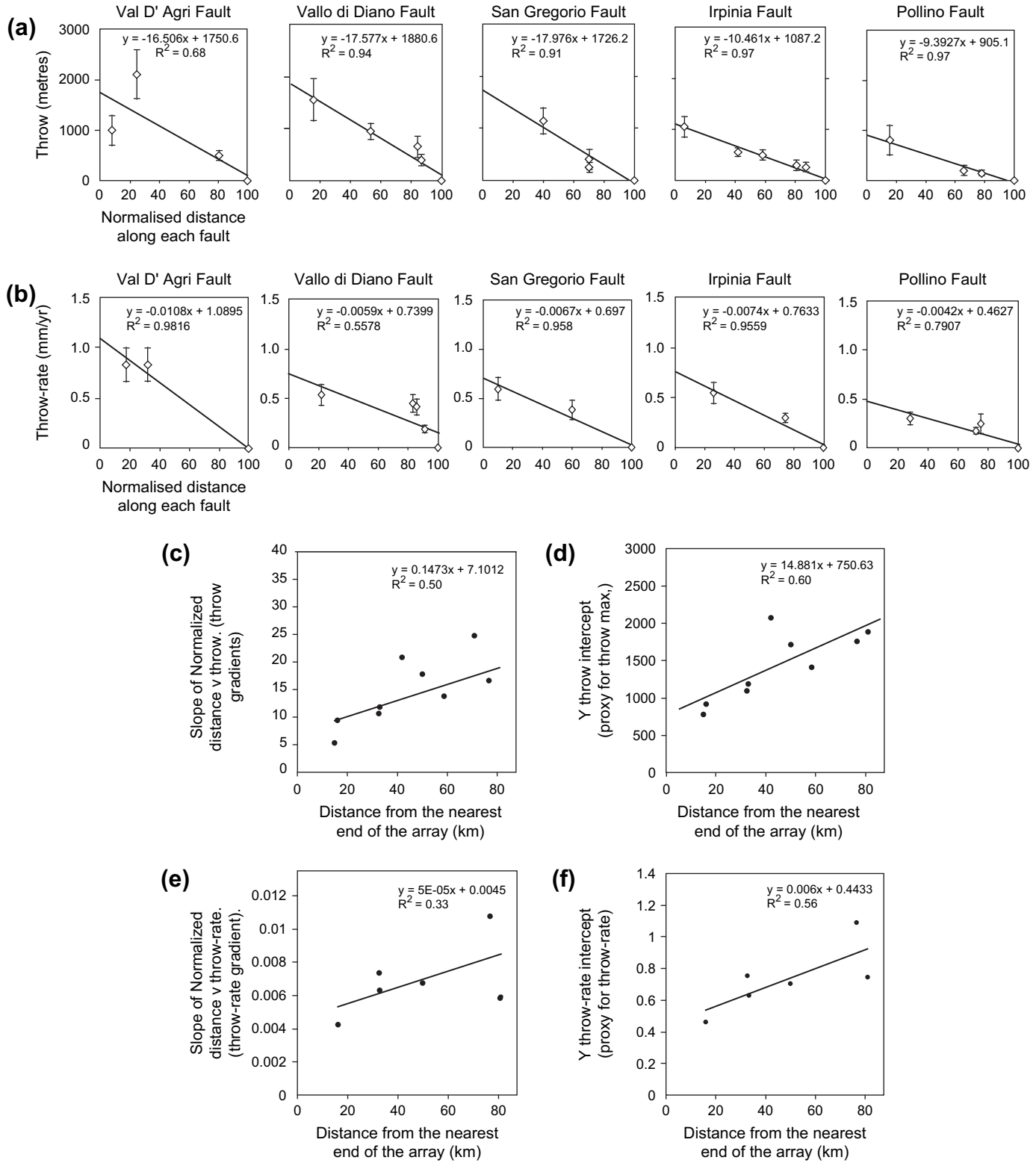

Fig. 12. (a) Plots of throw versus normalised distance from the centres of individual faults for the southern Apennines. (b) Plots of throw-rate versus normalised distance from the centres of individual faults. (c) Plot showing how the slopes of regression lines through the plots in (a) (throw-gradients) vary along the strike of the overall fault system. (d) Plot showing how the *y*-intercepts of regression lines through the plots in (a) (proxies for the throw maxima) vary along the strike of the overall fault system. (e) Plot showing how the slopes of regression lines through the plots in (b) (throw-rate-gradients) vary along the strike of the overall fault system. (f) Plot showing how the *y*-intercepts of regression lines through the plots in (b) (proxies for the throw-rate maxima) vary along the strike of the overall fault system.

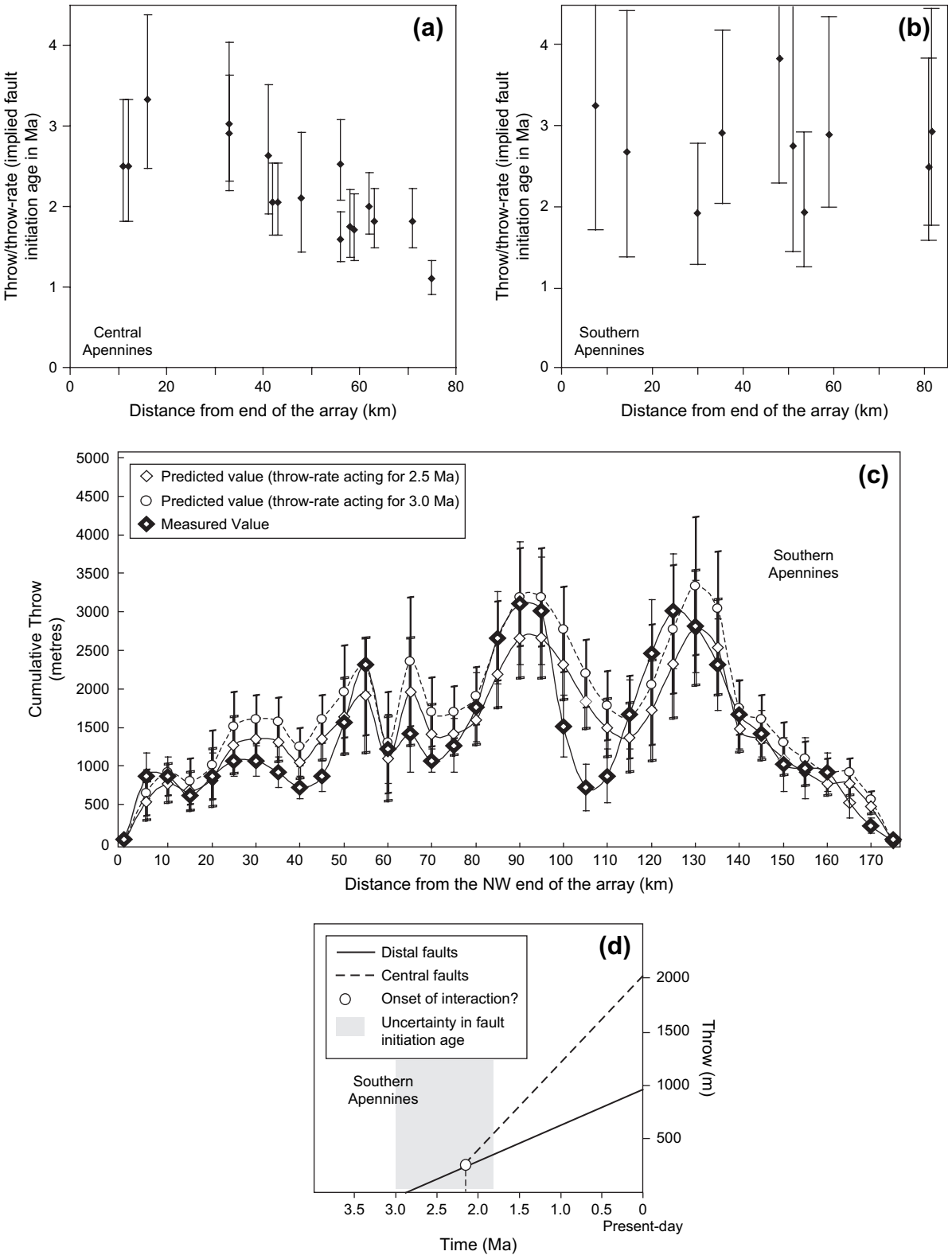

Fig. 13. (a) Plot of throw/throw-rate versus distance along the overall fault array for the central Apennines (Roberts and Michetti, 2004). (b) Plot of throw/throw-rate versus distance along the overall fault array for the southern Apennines. (c) Plot of cumulative throw summed across strike against distance along the strike of the fault system in the southern Apennines (compare with Fig. 1e for the central Apennines). Also shown are throws that would develop if throw rates measured from the southern Apennines were allowed to run for 3.0 and 2.5 Myrs. (d) Plot of throw versus time calculated using the present-day throw rates on the Pollino and Val d'Agri faults (data from Fig. 8; compare with Fig. 1f for the central Apennines).

Table 2
Predicted and measured throw–rates

Fault	L_i	$2R_i$	$2R_i/L_i$	Norm.	I.V.	50% <Overlap and Spacing<15 km	M.F.	Predicted value (mm/yr)	Measured value (mm/yr)
Volturara	30	30	1.00	0.27	0.22	None	1.0	0.22	0.30
Irpinia	31	65	2.10	0.56	0.47	None	1.0	0.47	0.54
San Gregorio	20	100	5.00	1.34	1.12	Alburni (13 km spacing)	0.5	0.56	0.59
Alburni	25	117	4.68	1.25	1.04	San Gregorio (13 km spacing)	0.5	0.52	0.39
Vallo di Diano	45	161	3.58	0.96	0.80	None	1.0	0.80	0.54
Val D'Agri	41	153	3.73	1.00	0.83	None	1.0	0.83	0.83
Maratea	38	88	2.32	0.62	0.52	None	1.0	0.52	0.43
Monte Alpi	33	104	3.15	0.84	0.70	None	1.0	0.70	0.55
Mercure	32	66	2.06	0.55	0.46	None	1.0	0.46	0.37
Pollino	32	32	1.00	0.27	0.22	None	1.0	0.22	0.30

L_i, the length of the fault; R_i, the distance from the fault midpoint to the nearest end of the fault array; Norm, normalised value, I.V., initial value prior to consideration of across strike interaction; M.F., modification factor (if a fault does not overlap more than 50% with a neighbouring fault and located more than 15 km away from the nearest fault the factor is 1.0, if 2 faults are within 15 km across strike and overlap by 50% then the factor is 0.5). Measured values represent throw-rates extracted from scarp profiles and published trench site data.

faults (Cowie and Roberts, 2001). Such patterns develop even where there is no gradient in far-field tectonic strain (Cowie, 1998), so there is no need to appeal to this for an explanation of this phenomenon. The driving mechanism has been argued to be Coulomb stress transfer during earthquakes, which drive faults located centrally within fault systems to slip more rapidly than distal faults, because they are at the centre of symmetry of multi-seismic-cycle stress transfer (Cowie and Roberts, 2001; Fig. 1). If this is correct, there must be a critical fault length/spacing relationship that evolves during fault growth. Early in the faulting history (Stage 1, Fig. 1b), faults may be too small, and too widely spaced for earthquakes to trigger slip on neighbouring faults. Thus, there is no reason why central faults should slip fastest given spatially uniform extension rate boundary conditions. As changes in the Coulomb failure function during normal faulting earthquakes extend for distances of several fault lengths away from the ruptured fault (Hodgkinson et al., 1996; Caskey and Wesnousky, 1997), the critical fault length/spacing will reflect this length scale. As faults grow across this threshold and begin to interact (Stage 2, Fig. 1b), central faults will accelerate. Thus, if Coulomb stress transfer does drive spatial slip-rate variations, then it is inevitable that slip rates will not be constant through time (Fig. 1). The critical question is therefore not whether slip rates can increase or remain constant during fault growth, but how fast faults make the transition from being too small to interact with their neighbours, to achieving the critical size where an earthquake on a fault can influence the Coulomb stress on a neighbour and cause fault interaction. Several studies have suggested that faults achieve their final lengths very rapidly, within a few percent of their total displacement history (Walsh et al., 2002; Nicol et al., 2005); this may explain why one cannot resolve very early throw-rate changes in southern Italy and elsewhere. Also, if fault systems have initial geometries where faults are distributed across strike, negative Coulomb-stress-driven feedback may inhibit rapid localisation, perhaps explaining why central Italy showed interaction-driven throw-rate acceleration late in its faulting history. With the inherent difficulties in resolving early syn-rift stratigraphy and timing for all fault systems, it may be that we have to turn to geomorphic indicators on immature fault systems or numerical models to study the early history of fault growth, and assess the controls on spatial variations in slip rate.

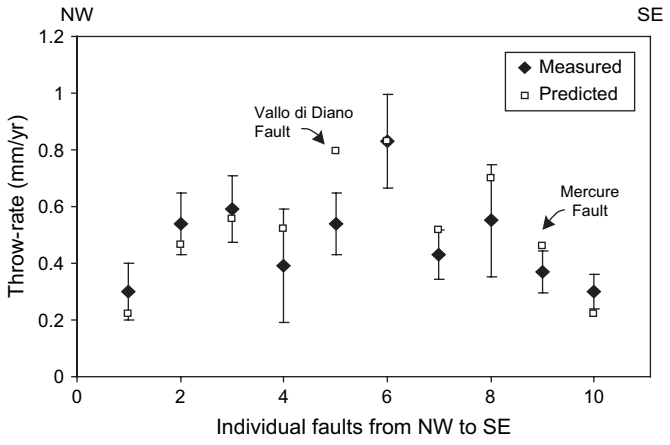

Fig. 14. Bar chart showing measured throw-rate maxima for individual faults in the southern Apennines alongside those predicted by the relationship $E = 2R_i/L_i$ explained in Section 8. The measured and predicted rates compare well suggesting the former are sensible values given knowledge of the comparative lengths of L_1 and L_2 faults.

10. Conclusions

We studied a localised, 175 km-long soft-linked normal fault system within the southern Apennines, accommodating extension towards 230.6° ± 3.9°. A profile of summed extension rate averaged since 18 ka shows a maxima of 1.1 ± 0.25 mm/yr, assuming 45° fault dips, decreasing to zero at the ends of the fault system; a profile of summed extension across the same faults shows a maxima of 3100 ± 700 m. Extension is at right-angles to the NW-SE striking fault system, indicating almost pure dip–slip motions. Oblique extension occurs locally near fault tips produced by strains associated with the

throw-gradients on the faults. Central faults have higher throws, and throw rates (2100 ± 500 m; 0.83 ± 0.15 mm/yr) than distal faults (800 ± 300 m; 0.3 ± 0.1 mm/yr), with values changing systematically along the strike of the fault system. When summed throw rates are allowed to run for 2.5–3.0 Myrs, the predicted throws are comparable to the measured values, suggesting that throw rates have been constant within the resolution of the data.

These characteristics are similar to those for the central Apennines (Roberts and Michetti, 2004), except that for latter, faulting is distributed across strike, and throw rates have increased by a factor of 6 late in the faulting history (75% elapsed time), at a time when other faults across strike became inactive in the mid-Pleistocene (Roberts et al., 2002). The areas share the same tectonic boundary conditions and lithospheric structure so this cannot explain the differences. We suggest that fault interaction is responsible for the differences.

If fault interaction is driven by Coulomb stress changes, where rupture of one fault brings its along strike neighbours closer to failure and across strike neighbours away from failure, it is inevitable that early in the history of faulting, when faults are too small to interact in this way, central faults will not necessarily be driven to fail more often than distal faults. Thus, when faults grow to a size that allows interaction, slip rates on central faults will increase relative to the distal faults, eventually producing profiles of total throw that adhere to global scaling relationships between throw and length. If rheological constraints cause fault systems to localise early in their histories, it will be difficult to resolve slip-rate changes using syn-rift stratigraphy unless temporal resolution is of order of a few percent of the total elapsed time of faulting. This uncertainty is important, because slip-rate histories on normal fault systems are a fundamental constraint on the mechanics of continental extension because they provide a timescale for such processes.

Acknowledgements

Funding was from the State Scholarship Foundation of Greece (IKY) (I.D.P.), NERC GR9/02995, NERC NE/B504165/1, and Birkbeck College (G.P.R.). Benfield Hazard Research Centre is acknowledged for support. Maria Papanikolaou and Eleni Kotsoni are thanked for assistance during fieldwork. We thank Alessandro Michetti, Eutizio Vittori, Nigel Morewood, Patience Cowie, Greg Tucker and Alex Whittaker for discussions concerning this study, and John Walsh and an anonymous referee for their reviews.

References

Allen, J.R.M., Brandt, U., Brauer, A., Hubberten, H.W., Huntley, B., Keller, J., Kraml, M., Mackensen, A., Mingram, J., Negendank, J.F.W., Nowaczyk, N.R., Oberhansli, H., Watts, W.A., Wulf, S., Zolitschka, B., 1999. Rapid environmental changes in southern Europe during the last glacial period. Nature 400, 740–743.

Amato, A., Montone, P., 1997. Present-day stress field and active tectonics in southern peninsular Italy. Geophysical Journal International 130, 519–534.

Amato, A., Montone, P., Cesaro, M., 1995. State of stress in Southern Italy from borehole breakout and focal mechanism data. Geophysical Research Letters 22, 3119–3122.

Anderson, H., Jackson, J., 1987. Active tectonics of the Adriatic region. Geophysical Journal of the Royal Astronomical Society 91, 937–983.

Anzidei, M., Baldi, P., Casula, G., Galvani, A., Mantovani, E., Pesci, A., Riguzzi, F., Serpelloni, E., 2001. Insights into present-day crustal motion in the central Mediterranean area from GPS surveys. Geophysical Journal International 146, 98–110.

Ascione, A., Romano, P., 1999. Vertical movements on the eastern margin of the Tyrrhenian extensional basin. New data from the Mt. Bulgheria (Southern Apennines, Italy). Tectonophysics 315, 337–356.

Ascione, A., Cinque, A., Improta, L., Villani, F., 2003. Late Quaternary faulting within the Southern Apennines seismic belt: new data from Mt. Marzano area (Southern Italy). Quaternary International 101–102, 27–41.

Avouac, J.P., 1993. Analysis of scarp profiles: evaluation of errors in morphologic dating. Journal of Geophysical Research 98, 6745–6754.

Barchi, M., Amato, A., Cippitelli, G., Merlini, S., Montone, P. Extensional tectonics and seismicity in the axial zone of the Southern Apennines. Boll. Soc. Geol. It, in press.

Bartole, R., Savelli, C., Tramontana, M., Wezel, F.C., 1984. Structural and sedimentary features in the Tyrrhenian margin of Campania, Southern Italy. Marine Geology 55, 163–180.

Benedetti, L., Tapponnier, P., King, G.C.P., Piccardi, L., 1998. Surface rupture of the 1857 southern Italian earthquake? Terra Nova 10, 206–210.

Bernard, P., Zollo, A., 1989. The Irpinia, 1980 earthquake: detailed analysis of a complex normal faulting. Journal of Geophysical Research 94, 1631–1647.

Blumetti, A.M., Esposito, E., Ferreli, L., Michetti, A.M., Porfido, S., Serva, L., Vittori, E., 2003. New data and reinterpretation on the November 23, 1980, M 6.9 Irpinia-Lucania earthquake (Southern Apennines) coseismic surface effects. In: Dramis, F., Farabollini, P., Molin, P. (Eds.), Large scale vertical movements and related gravitational processes. Study Geologici Camerti special issue, 2002, pp. 19–27.

Boschi, E., Ferrari, G., Gasperini, P., Guidoboni, E., Smriglio G., Valensise, G., 1995. Catalogo dei forti terremoti in Italia dal 461 a.C. al, 1980, Istituto Nazionale di Geofisica—SGA Storia Geofisica Ambiente, printed by Grafica Ragno, Ozzano Emilia, BO, Italy, 973 p.

Butler, R.W.H., Mazzoli, S., Corrado, S., DeDonatis, M., DiBucci, D., Gambini, R., Naso, G., Nicolai, C., Scrocca, D., Shiner, P., Zucconi, V., 2004. Applying thick-skinned tectonic models to the Apennine thrust belt of Italy—Limitations and implications. In: McClay, K.R. (Ed.), Thrust tectonics and hydrocarbon systems: AAPG Memoir 82, pp. 647–667.

Cartwright, J.A., Trudgill, B.D., Mansfield, C.S., 1995. Fault growth by segment linkage: An explanation for scatter in maximum displacement and trace length data from the Canyonlands Grabens of SE Utah. Journal of Structural Geology 17, 1319–1326.

Caskey, S.J., Wesnousky, S.G., 1997. Static stress changes and earthquake triggering during the 1954 Fairview Peak and Dixie Valley earthquakes, Central Nevada. Bulletin of the Seismological Society of America 87, 521–527.

Cavinato, G.P., De Celles, P.G., 1999. Extensional basins in the tectonically bimodal central Apennines fold-thrust belt, Italy: Response to corner flow above a subducting slab in retrograde motion. Geology 27, 955–958.

Cavinato, G.P., Carusi, C., Dall'Asta, M., Miccadei, E., Piacentini, T., 2002. Sedimentary and tectonic evolution of Plio-Pleistocene alluvial and lacustrine deposits of the Fucino Basin (central Italy). Sedimentary Geology 148, 29–59.

Cello, G., Mazzoli, S., Tondi, E., Turco, E., 1997. Active tectonics in the Central Apennines and possible implications for seismic hazard analysis in peninsular Italy. Tectonophysics 272, 43–68.

Chevalier, F., Guiraud, M., Garcia, J.-P., Dommergues, J.-L., Quesne, D., Allemand, P., Dumont, T., 2003. Calculating the long-term displacement rates of a normal fault from the high-resolution stratigraphic record (early Tethyan rifting, French Alps). Terra Nova 15 (6), 410–416.

Cinti, F., Cucci, L., Pantosti, D., D'Addezio, G., Meghraoui, M., 1997. A major seismogenic fault in a "silent area": the Castrovillari fault (southern Italy). Geophysical Journal International 130, 595–605.

Cinti, F.R., Moro, M., Pantosti, D., Cucci, L., D'Addezio, G., 2002. New constraints on the seismic history of the Castrovillari fault in the Pollino gap (Calabria, southern Italy). Journal of Seismology 6, 199–217.

Cinque, A., Ascione, A., Caiazzo, C., 2000. Distribuzione spazio-temporale e caratterizzazione della fagliazione quaternaria in Appennino meridionale. In: Galdini, F., Meletti, C., Rebez, A. (Eds.), Le ricerche del GNDT nel campo della pericolosita sismica (1996–1999). CNR-GNDT, Roma, pp. 107–136.

CNR, 1990. Structural model of Italy, 1:500000. In: Bigi, G., Cosentino, D., Parotto, M., Sartori, R., Scandone, P. (Eds.), Consiglio Nazionale delle Richerche. S.E.L.C.A., Florence.

Cocco, M., Pacor, F., 1993. The rupture process of the, 1980 Irpinia, Italy, earthquake from the inversion of strong motion waveforms. Tectonophysics 218, 157–177.

Collela, A., Lapenna, V., Rizzo, E., 2004. High-resolution imaging of the High Agri Valley Basin (Southern Italy) with electrical resistivity tomography. Tectonophysics 386, 29–40.

Corrado, S., Invernizzi, C., Mazzoli, S., 2002. Tectonic burial and exhumation in a foreland fold and thrust belt: the Monte Alpi case history (Southern Apennines, Italy). Geodinamica Acta 15, 159–177.

Cowie, P.A., 1998. A healing-reloading feedback control on the growth rate of seismogenic faults. Journal of Structural Geology 20, 1075–1087.

Cowie, P.A., Roberts, G.P., 2001. Constraining slip rates and spacings for active normal faults. Journal of Structural Geology 23, 1901–1915.

Cowie, P.A., Underhill, J.R., Behn, M.D., Lin, J.L., Gill, C.E., 2005. Spatio-temporal evolution of strain accumulation derived from multi-scale observations of late Jurassic rifting in the northern North Sea: A critical test of models for lithospheric extension. Earth and Planetary Science Letters 234, 401–419.

D'Agostino, N., Jackson, J.A., Dramis, F., Funiciello, R., 2001. Interactions between mantle upwelling, drainage evolution and active normal faulting: an example from the central Apennines (Italy). Geophysical Journal International 147, 475–497.

D'Addezio, G., Pantosti, D., Valensise, G., 1991. Paleoearthquakes along the Irpinia fault at Pantano di San Gregorio Magno (Southern Italy). Il Quaternario 4, 121–136.

Di Bucci, D., Naso, G., Corrado, S., Villa, I.M., 2005. Growth, interaction and seismogenic potential of coupled active normal faults (Isernia Basin, central-southern Italy). Terra Nova 17, 44–55.

Di Bucci, D., Massa, B., Zuppetta, A., 2006. Relay ramps in active normal fault zones: A clue to the identification of seismogenic sources (1688 Sannio earthquake, Italy). GSA Bulletin 118, 430–448.

Doglioni, C., Harabaglia, P., Martinelli, G., Mongelli, F., Zito, G., 1996. A geodynamic model of the Southern Apennines accretionary prism. Terra Nova 8, 540–547.

Ferranti, L., Oldow, J.S., Sacchi, M., 1996. Pre-Quaternary orogen-parallel extension in the Southern Apennine belt, Italy. Tectonophysics 260, 325–347.

Galadini, F., Messina, P., 2004. Early-Middle Pleistocene eastward migration of the Abruzzi Apennine (central Italy) extensional domain. Journal of Geodynamics 37, 57–81.

Gattacceca, J., Speranza, F., 2002. Paleomagnetism of Jurassic to Miocene sediments from the Apenninic carbonate platform (southern Apennines, Italy): evidence for a 60° counterclockwise Miocene rotation. Earth and Planetary Science Letters 201, 19–34.

Giraudi, C., 1995. I detriti di versante al margin della piana del Fucino (Italia centrale): significato palaeoclimatico ed impatto antropico. Il Quaternario 8, 203–210.

Hippolyte, J.C., Angelier, J., Roure, F., 1994. A major geodynamic change revealed by Quaternary stress patterns in the South Apennines (Italy). Tectonophysics 230, 199–210.

Hippolyte, J.C., Angelier, J., Barrier, E., 1995. Compressional and extensional tectonics in an arc system: example of the Southern Apennines. Journal of Structural Geology 17, 1725–1740.

Hodgkinson, K.M., Stein, R.S., King, G.C.P., 1996. The 1954 Rainbow Mountain-Fairview Peak-Dixie Valley earthquakes: a triggered normal faulting sequence. Journal of Geophysical Research 101, 25459–25471.

Hunstad, I., Selvaggi, G., D'Agostino, N., England, P., Clarke, P., 2003. Pierozzi, M., Geodetic strain in peninsular Italy between 1875 and, 2001, 2003. Geophysical Research Letters 30, 1181, doi:10.1029/2002GL016447.

Jackson, J.A., White, N.J., 1989. Normal faulting in the upper continental crust: observations from regions of active extension. Journal of Structural Geology 11, 15–36.

Knott, S.D., Turco, E., 1991. Late Cenozoic kinematics of the Calabrian arc, Southern Italy. Tectonics 10, 1164–1172.

Lucente, F.P., Chiarabba, C.G., Cimini, B., 1999. Tomographic constraints on the geodynamic evolution of the Italian region. Journal of Geophysical Research 104, 20,307–20,327.

Margheriti, L., Lucente, F.P., Pondrelli, S., 2003. SKS splitting measurements in the Apenninic-Tyrrhenian domain (Italy) and their relation with lithospheric subduction and mantle convection. Journal of Geophysical Research 108 (B4), 2218, doi:10.1029/2002JB001793.

Malinverno, A., Ryan, W.B.F., 1986. Extension in the Tyrrhenian sea and shortening in the Apennines as result of the arc migration driven by sinking of the lithosphere. Tectonics 5, 227–245.

Maschio, L., Ferranti, L., Burrato, P., 2005. Active extension in Val' d'Agri area, Southern Apennines, Italy: implications for the geometry of the seismogenic belt. Geophysical Journal International 162, 591–609.

McLeod, A., Dawers, N.H., Underhill, J.R., 2000. The propagation and linkage of normal faults: insights from the Strathspey-Brent-Statfjord fault array, northern North Sea. Basin Research 12 (263–284), 2000.

Meyer, V., Nicol, A., Childs, C., Walsh, J., Watterson, J., 2002. Progressive localisation of strain during the evolution of a normal fault population. Journal of Structural Geology 24, 1215–1231.

Michetti, A.M., Ferreli, L., Serva, L., Vittori, E., 1997. Geological evidence for strong historical earthquakes in an "aseismic" region: the Pollino case (Southern Italy). Journal of Geodynamics 24 (1–4), 67–86.

Michetti, A.M., Ferreli, L., Esposito, E., Porfido, S., Blumetti, A.-M., Vittori, E., Serva, L., Roberts, G.P., 2000. Ground effects during the 9 September, 1998, M_w=5.6, Lauria earthquake and the seismic potential of the "Aseismic" Pollino region in Southern Italy. Seismological Research Letters 71, 31–46.

Minissale, A., 2004. Origin, transport and discharge of CO_2 in central Italy. Earth Science Reviews 66, 89–141.

Monaco, C., Tortorici, L., Paltrinieri, W., 1998. Structural evolution of the Lucanian Apennines, southern Italy. Journal of Structural Geology 20, 617–638.

Mostardini, F., Merlini, S., 1986. Appennino centro meridionale, sezioni geologiche e proposta di modello strutturale. Memorie della Societa Geologica Italiana 35, 177–202.

Nicol, A., Walsh, J.J., Watterson, J., Underhill, J., 1997. Displacement rates of normal faults. Nature 390, 157–159.

Nicol, A., Walsh, J.J., Berryman, K., Nodder, S., 2005. Growth of a normal fault by the accumulation of slip over millions of years. Journal of Structural Geology 27, 327–342.

Nocquet, J.-M., Calais, E., 2004. Geodetic measurements of crustal deformation in the Western Mediterranean and Europe. Pure Applied Geophysics 161, 661–681.

Noguera, A.M., Rea, G., 2000. Deep structure of the Campanian-Lucanian Arc (Southern Apennine, Italy). Tectonophysics 324, 239–265.

Oldow, J.S., D'Argenio, B., Ferranti, L., Pappone, G., Marsella, E., Sacchi, M., 1993. Large-scale longitudinal extension in the southern Apennines contractional belt, Italy. Geology 21, 1123–1126.

Palmentola, G., Acquafredda, P., Fiore, S., 1990. A new correlation of the Glacial Moraines in the Southern Apennines, Italy. Geomorphology 3, 1–8.

Palumbo, L., Benedetti, L., Bourles, D., Cinque, A., Finkel, R., 2004. Slip history of the Magnola fault (Apennines, Central Italy) from 36Cl surface exposure dating: evidence for strong earthquakes over the Holocene. Earth Planetary Science Letters 225, 163–176.

Pantosti, D., Valensise, G., 1990. Faulting mechanism and complexity of the November 23, 1980, Campania-Lucania earthquake, inferred from surface observations. Journal of Geophysical Research 95, 15319–15341.

Pantosti, D., Schwartz, D.P., Valensise, G., 1993. Paleoseismology along the, 1980 surface rupture of the Irpinia fault: implications for the Earthquake

recurrence in the Southern Apennines, Italy. Journal of Geophysical Research 98, 6561–6577.

Papanikolaou, I.D., 2003. Generation of high-resolution seismic hazard maps in extensional tectonic settings through integration of earthquake geology, fault mechanics theory and GIS techniques. Unpublished PhD thesis, University of London.

Papanikolaou, I.D., Roberts, G.P., Michetti, A.M., 2005. Fault scarps and deformation rates in Lazio-Abruzzo, Central Italy: Comparison between geological fault slip-rate and GPS data. Tectonophysics 408, 147–176.

Patacca, E., Sartori, R., Scandone, P., 1990. Tyrrhenian Basin and Apenninic Arcs: Kinematic relations since late Tortonian times. Mem. Soc. Geol. It 45, 425–451.

Piccardi, L., Gaudemer, Y., Tapponier, P., Boccaletti, M., 1999. Active oblique extension in the central Apennines (Italy): evidence from the Fucino region. Geophysical Journal International 139, 499–530.

Porfido, S., Esposito, E., Vittori, E., Tranfaglia, G., Michetti, A.M., Blumetti, A.M., Ferreli, L., Guerrieri, L., Serva, L., 2002. Aerial distribution of ground effects induced by strong earthquakes in the southern Apennines (Italy). Surveys in Geophysics 23, 529–562.

Roberts, G.P., 1996. Variation in fault-slip directions along active and segmented normal fault systems. Journal of Structural Geology 18, 835–845.

Roberts, G.P., Ganas, A., 2000. Fault-slip directions in central-southern Greece measured from striated and corrugated fault planes: comparison with focal mechanism and geodetic data. Journal of Geophysical Research 105, 23,443–23,462.

Roberts, G.P., Michetti, A.M., 2004. Spatial and temporal variations in growth rates along active normal fault Systems: an example from Lazio-Abruzzo, central Italy. Journal of Structural Geology 26, 339–376.

Roberts, G.P., Michetti, A.M., Cowie, P., Morewood, N.C., Papanikolaou, I., 2002. Fault slip-rate variations during crustal-scale strain localisation, central Italy. Geophysical Research Letters 29 (8), doi:10.1029/2001GL013529. 2002.

Royden, L., Patacca, E., Scandone, P., 1987. Segmentation and configuration of subducted lithosphere in Italy: An important control on thrust belt and foredeep basin evolution. Geology 15, 714–717.

Schlische, R.W., Young, S.S., Ackermann, R.V., Gupta, A., 1996. Geometry and scaling relations of a population of very small rift-related faults. Geology 24, 683–686.

Selvaggi, G., Castello, B., Azzara, R., 1997. Spatial distribution of scalar seismic moment release in Italy (1983–1996): seismotectonic implications for the Apennines. Annali di Geofisica 40, 1565–1578.

Servizio Geologico D'Italia, 1969a. Carta Geologica d'Italia 1:100,000 Potenza.

Servizio Geologico D'Italia, 1969b. Carta Geologica d'Italia 1:100,000 Salerno.

Servizio Geologico D'Italia, 1970a. Carta Geologica d'Italia 1:100,000 Verbicaro.

Servizio Geologico D'Italia, 1970b. Carta Geologica d'Italia 1:100,000 Lauria.

Servizio Geologico D'Italia, 1970c. Carta Geologica d'Italia 1:100,000 S. Angelo de'Lombardi.

Servizio Geologico D'Italia, 1970d. Carta Geologica d'Italia 1:100,000 Eboli.

Servizio Geologico D'Italia, 1971. Carta Geologica d'Italia 1:100,000 Castrovillari.

Speranza, F., Mattei, M., Naso, G., Di Bucci, D., Corrado, S., 1998. Neogene-Quaternary evolution of the central Apennine orogenic system (Italy): a structural and palaeomagnetic approach in the Molise region. Tectonophysics 299, 143–157.

Taylor, S.K., Bull, J.M., Lamarche, G., Barnes, P.M., 2004. Normal fault growth and linkage in the Whakatane Graben, New Zealand, during the last 1.3 Myr. Journal of Geophysical Research 109, B02408, doi:10.1029/2003JB002412.

Tortorici, L., Monaco, C., Tansi, C., Cocina, O., 1995. Recent and active tectonics in the Calabrian arc (Southern Italy). Tectonophysics 243, 37–55.

Van Dijk, J.P., Bello, M., Toscano, C., Bersani, A., Nardon, S., 2000. Tectonic model and three-dimensional fracture network analysis of Monte Alpi (southern Apennines). Tectonophysics 324, 203–237.

Vittori, E., Ferreli, L., Michetti, A.M., Serva, L., 1995. Holocene paleoearthquakes along the Pollino fault zone (Northern Calabria, Italy): inplications for seismic hazard assessment. In: Proceedings of the Fifth International Conference on Seismic Zonation, Nice. Quest Editions Presses Academiques, pp. 1400–1407. October 17–19/1995.

Walsh, J.J., Childs, C., Meyer, V., Manzocchi, T., Imber, J., Nicol, A., Tuckwell, G., Bailey, W.R., Bonson, C.G., Watterson, J., Nell, P.A.R., Strand, J.A., 2001. Geometrical controls on the evolution of normal fault systems. In: Holdsworth, R.E., Strachan, R.A., Magloughlin, J.F., Knipe, R.J. (Eds.), The Nature of the Tectonic Significance of Fault Zone Weakening. Geological Society of London, Special Publication 186, pp. 157–170.

Walsh, J.J., Nicol, A., Childs, C., 2002. An alternative model for the growth of faults. Journal of Structural Geology 24, 1669–1675.

Westaway, R., 1987. The Campania, southern Italy, earthquakes of, 1962 August 21. Geophysical Journal of the Royal Astronomical Society 88, 1–24.

Westaway, R., 1992. Seismic Moment Summation for Historical Earthquakes in Italy: Tectonic Implications. Journal of Geophysical Research 97, 15437–15464.

Westaway, R., 1993. Quaternary uplift of Southern Italy. Journal of Geophysical Research 98, 21741–21772.

Westaway, R., Jackson, J., 1987. The earthquake of 1980 November 23 in Campania-Basilicata (southern Italy). Geophysical Journal of the Royal Astronomical Society 90, 375–443.

Yeats, R.S., Sieh, K., Allen, C.R., 1997. The Geology of Earthquakes. Oxford University Press, New York.